

Kirschner, F.

721398

4.2.2

BCC

7-96-01
II - A - 859

F-2-7

THE 6TH INTERNATIONAL CONGRESS ON ACOUSTICS
TOKYO, JAPAN, AUGUST 21-28, 1968

Control of Railroad Wheel Screech Noise

Francis Kirschner

Director of Engineering

The Soundcoat Company, Inc.

Introduction

The screech noise generated by railroad wheels on sharp curves has been a source of discomfort since the introduction of railroads. The control of this noise source has been attempted with many auxiliary treatments, such as lubrication of the rails; vibration isolators between the shaft and the shoe of the wheel, but their safety and cost-effectiveness have not been fully acceptable. There is also an approach which applied a lead ring around the rim of the wheel, and Stuber (Ref. 1) applied 10mm thick rubber coatings to both sides of the web of the wheel in order to obtain noise reduction. Since 1963 efforts have been made in the U.S. to apply the newly developed, high efficiency, visco-elastic materials for the suppression of screech noise, first on model wheels, then in laboratory experiments, and finally in field trials.

From the acoustician's point of view, the railroad wheel is like a bell or a loud speaker with well defined nodal lines of vibration, and its radiation effectiveness is well demonstrated, as screech noise

n dB A

with dif-
s mea-
son the

asoning
cted in
he ap-
ere
was

ction
ed in

a on
leula-

d be-
in

in
is,
oints

num-
d

acco-
o de-
to

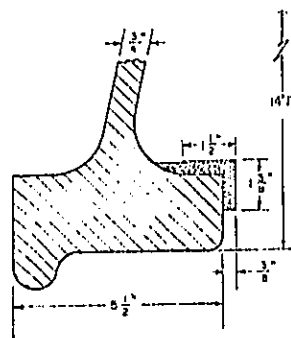
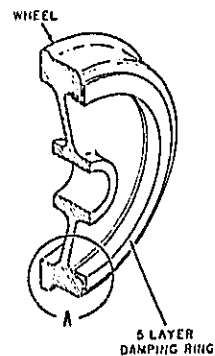
pe-

721398

721398



can be heard for distances of over a mile. From the noise control engineer's point of view, the steel railroad wheel most popular in the United States is a 28" diameter, 550 lb. (220 kg) steel forging with a variable cross-section, shown on the attached figure 1, being as wide as 5½" at the shoe of the wheel. The temperature of the wheel under normal running conditions can rise on high speed trains to 180-200°F. with dynamic braking and for short periods of time up to 400°F. in emergency braking conditions. Lateral space allowed for damping treatment as additional thickness at the rim has to be thin enough to clear signal systems, frog switches and routine maintenance and machine operations required in regrinding of flat wheels.



DETAIL A
(Figure 1)

A thorough study of these conditions was made first in the laboratory, and the following design goals have been established based on numerous field trials in the yards of the Toronto Transit Commission (TTC) for the homogeneous treatment and at the Port of Authority of New York Trans-Hudson Corporation (PATH) system for this new vibration damping treatment for which we list the following design goals:

- A) At least 24 db. reduction in screech noise (for all practical purposes will make the screech noise inaudible in comparison to the

rol
in
ging
being



amping
tical
the

running noise of the car); B) Damping treatment weight not to exceed 4% of the weight of the wheel (550 lbs. wheel) - (< 22 lbs. Damping Treatment). C) Thickness of treatment in width of rim less than 3/8". D) The bond strength sufficient for safety and structural integrity of the treatment at the temperature extremes. E) The damping material



(Figure 2)

must have a high stiffness constant to maintain the integrity and safety of the structure for high centrifugal accelerations at wide temperature extremes. In order to obtain maximum damping efficiency in minimum space and weight, we developed a five-layer ring which is effective over the whole audible frequency spectrum. Thus, excellent damping is obtained for the high modes of vibration, rather than only for the relatively small damping and loss factors which can be obtained with the three-layer system (Ref. 2). In addition, from the mechanical point of view, we know that for a ring configuration, the constraining layer does not shift the position of the neutral axis in the right position for maximum damping (Ref. 3). We have split our ring treatment, which allows us to take advantage of the extensional and shear damping as well, and provides a very effective non-linear damping system (Fig. 1), because of the large elliptical deformation during vibration in the steel wheels (Fig. 2).

Noise Reduction Results

The noise reduction obtained in field trials is given (Fig. 3), for a five-layer damping treatment, which meets all our design goals

in terms of weight, space limitations, temperature extremes and mechanical strengths. Noise levels with and without treatment on the sharpest curve available in the United States railroad industry (90 ft. radius at Hudson Terminal in New York), are illustrated for two untreated and two treated cars (with 16 wheels each) rounding

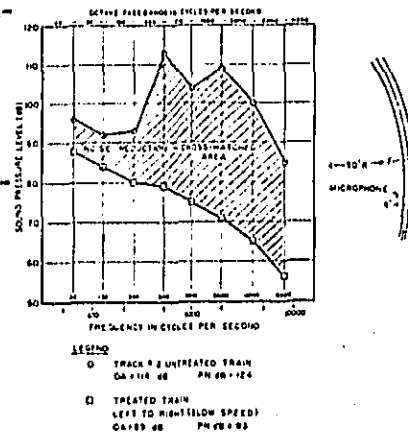


(Figure 3)

the 90 ft. radius curve. The amount of noise reduction in overall noise levels is 25 db. In PN db (Perceived Noise levels) untreated it is 125 PN db and with damping it is 93 PN db, or a reduction of 31 PN db. The noise reduction in the octave bands centered at 500 cycles is from 113 db to 79 db; and at the next highest screech peak in the 2000 CPS octave band, it is from 109 to 71 db. Tests were also run b) in the open and, c) in a tunnel where the highest noise levels can be expected due to the reverberations of the tunnel walls, and a similar noise reduction was confirmed in all three cases.

Ref. 1 -- Camill Stüber -- Beispiele zur Lärmabwehr bei der Deutschen Bundesbahn. Lärmbekämpfung, Heft 1/1965.

Ref. 2 -- DiTaranto and Blasingame -- Composite Loss Factors of Selected Laminated Beams. J.A.S.A.

Ref. 3 -- Vibration Damping Sandwich Configurations by Y. T. Yin, ASME Vibration Conference, Boston, Mass., 1967.

432281

890

November, 1972

TE 4

of Registration and Education, Division of Industrial Planning and Development, Springfield, Ill., 1958.
14. Wilbur Smith and Associates, Illinois Highway Administration Study, Vol. 1, Dec., 1966.
15. Wilbur Smith and Associates, Illinois Highway Needs and Fiscal Study, Final Report, Oct., 1967.

RECEIVED

JAN 26 1973

NOISE ABATEMENT PROGRAM
INFORMATICS INC.

*Need
SAL
RR (1-24-73)*

Mass transportation - Noise
9382 November, 1972 TE 4
4421

TRANSPORTATION ENGINEERING JOURNAL

Proceedings of the American Society of Civil Engineers

1298

NOISE AND VIBRATION CONTROL IN NEW RAPID TRANSIT

By Marshall L. Silver, A. M. ASCE

(Reviewed by the Urban Transportation Division)

get noted sub

INTRODUCTION

The transit passenger is a sophisticated individual who requires that his transportation mode be safe, reliable, cheap, convenient, and comfortable. The transportation designer and engineer have traditionally recognized some of these factors while overlooking others. For example, planners always are conscious of the importance of safety and reliability in any design that involves the public. Likewise, costs are always considered so that the system can be built and operated economically. New transportation technology is providing convenience to the passenger by eliminating waiting, transferring, parking and fare collection problems. On the other hand, passenger comfort was often overlooked by planners and engineers. The resulting uncomfortable transit environment was caused in part by a lack of knowledge concerning the importance of comfort because such considerations were not traditionally a part of the planning or design process.

In the newer transportation systems, engineers and designers have recognized the importance of comfort with the result that architectural appearance, correct lighting, and proper ventilation now receive great attention. Surprisingly however, control of excessive noise and vibration which may fatigue, reduce efficiency and annoy to a far greater degree than any of these other factors have largely been neglected.

One possible reason for this neglect is that the noise and vibration design process is difficult because the transportation specialist must consider the needs of three separate groups: the riding passenger, the waiting passenger, and the wayside community. The riding passenger wants low noise and vibration levels so that he may talk to his neighbor, read a newspaper in comfort,

Note.—Discussion open until April 1, 1973. To extend the closing date one month, a written request must be filed with the Editor of Technical Publications, ASCE. This paper is part of the copyrighted Transportation Engineering Journal of ASCE, Proceedings of the American Society of Civil Engineers, Vol. 98, No. TE4, November, 1972. Manuscript was submitted for review for possible publication on February 3, 1972.
¹Asst. Prof., Dept. of Materials Engrg., Univ. of Illinois, Chicago, Ill.

or simply relax. The passenger entering the transit station or waiting for a vehicle should not be subjected to an uncomfortable environment radically different from that outside the transportation facility if his continued ridership is sought. The unseen passenger, and the community do not want to be disturbed. Wayside residences should not be subjected to excessive noise or vibration levels nor should adjacent business feel that the transit system is interfering with trade. The needs of these three groups are often not compatible which forces the engineer and the designer to develop compromise solutions to noise and vibration problems that serve the common interests of all portions of the community.

The transportation planner and engineer can efficiently provide a pleasing transportation environment to the passenger and community only if he is aware of the factors that contribute to excess noise and vibration. In this way he will have the information necessary to develop the appropriate controls and to incorporate them into the design from the very beginning of the planning process where they are most effective and economical. With this goal in mind, the following pages will present information on current noise levels that exist in urban areas as well as summarize data describing noise and vibration levels generated by different components of existing transit systems. A summary of noise and vibration criteria currently being used by some of the major

TABLE 1.—TYPICAL COMMUNITY NOISE LEVELS OBSERVED IN METROPOLITAN AREA (13)

Type of area (1)	Type of noise (2)	Noise level, in dBA (3)
Quiet residential	Day background	40-50
	Night background	35-45
Average residential	Day background	50-60
	Night background	40-50
Semi-commercial residential	Day background	50-60
	Night background	45-55
Commercial	Day background	55-65
	Night background	45-55
Residential removed from freeways and boulevards	Autos	60-70
	Trucks	70-80
	Airplanes	60-70
	Freight trains	80-95
Residential near flight pattern	Airplanes	75-85
Residential-commercial or near boulevards	Autos	65-75
	Trucks	70-80
	Busses	70-80
	Airplanes	70-80
Sidewalk of commercial area	Autos	70-80
	Busses and Trucks	80-90
Industrial	Day background	60-70
	Night background	50-60
	Autos	65-75
	Trucks	75-85

transit operators will be presented to provide a basis for developing limiting noise and vibration formulas for a variety of transportation technologies.

COMMON ENVIRONMENTAL NOISE AND VIBRATION LEVELS

The urban environment is a noisy place and Fig. 1 represents the range of sound levels in decibels commonly encountered in daily urban activities. The decibel is the logarithm of the ratio of a measured sound pressure to a reference sound pressure. The starting point in the scale of noise levels (zero dB) is about the level of the weakest sound that can be heard by a person with very good hearing in an extremely quiet location. A reference sound pressure of 0.002 microbars is commonly used to fix the zero level because it is approximately the threshold of hearing at 1,000 cps.

The overall noise level is commonly reported as a sound pressure level, dB, and is recorded on a sound level meter operating with uniform frequency response characteristics. Another common noise measure is the sound level of a noise, dBA, which is measured with the sound level meter operating with a weighting network that gives a comparative sound level based on frequency. The A meter scale, having poor relative response to sounds at frequencies below about 500 cps, has been shown to be closely correlated with subjective interpretations of noise and is a useful single number measure of overall noise level.

Transportation systems are probably the biggest contributors to urban noise levels. This fact is hinted at in Fig. 1 and shown more closely in Table

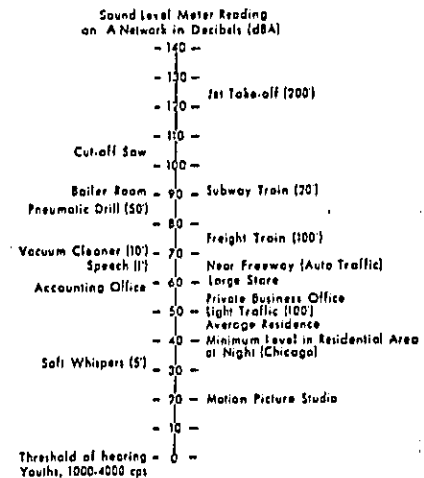


FIG. 1.—RANGE OF NOISE LEVELS COMMONLY ENCOUNTERED IN URBAN AREAS

1 which lists typical community noise levels observed in various metropolitan locations ranging from quiet residential neighborhoods to industrial areas (13). These noise levels average 45 dBA during the day and 40 dBA at night in the quietest residential neighborhoods increasing to levels of 60 dBA during the day in commercial areas. However, the bus and truck traffic can raise this level to 80 dBA in residential areas and to levels of 90 dBA along the sidewalks of commercial areas. These values, of course, do not consider the noise

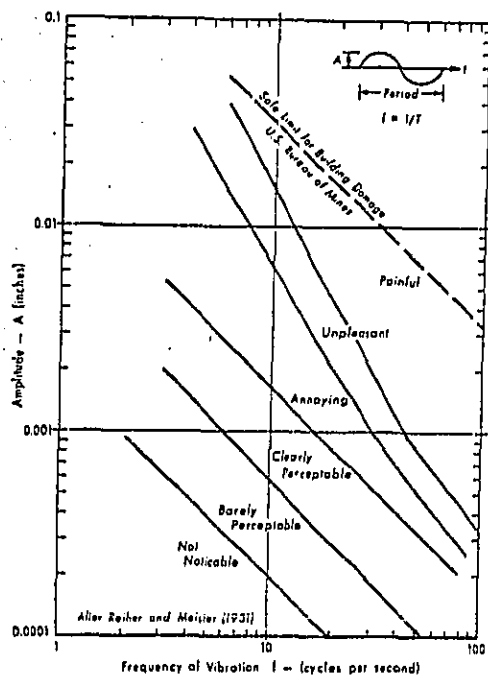


FIG. 2.—HUMAN SENSITIVITY LIMITS AND STRUCTURAL DAMAGE CRITERIA FOR VERTICAL VIBRATIONS OF SIMPLE HARMONIC FORM (16)

produced by an occasional vehicle with a defective muffler which would raise noise levels to an even higher level.

Ideally, building interior noise levels should be much lower than the levels commonly measured exterior to the building. For example, the Wilson Noise Study Committee (20) in England suggested that noise levels of 55 dBA in quiet offices and levels of 68 dBA in noisy offices should never be exceeded. In addition, the committee recommended that noise levels of 50 dBA during the

day and 35 dBA at night should not be exceeded for more than 10 % of the time. However, field measurements have shown that such noise levels are more often exceeded than maintained in a large number of urban offices and residences (20).

Urban awareness to vibration is generally restricted to locations where the existing vibration amplitudes are fairly high. Some individuals are subjected to excessive vibration levels in their work but the majority of the population is exposed to transportation generated vibration either in private automobiles or in rapid transit systems. Human response to vibration depends on the amplitude and the frequency of the motion as well as the psychological conditioning of the individual (6,7,8). Complicated interrelation of each of these factors makes it extremely difficult to develop one single measure that describes the subjective nature of vibration measurements.

One of the more useful descriptions of human tolerance to transportation vibration was provided by Reiter and Meiser (15) who subjected individuals to steady state vibrations in shaking table tests. Their measurements indicated that certain combinations of vibration amplitude were not noticeable to individuals while other combinations were troublesome or actually caused severe discomfort. The form of their results are shown in Fig. 2. Also plotted in Fig. 2 is the level of vibration generally thought to be the limit above which structural damage may occur. These levels are fairly high when compared to the vibration tolerance of people and were developed as criteria for safe blasting operation near structures.

Vibration levels generated by the operation of transit systems are nowhere near the levels generally required to cause structural distress. On the other hand, transit vehicles often cause troublesome vibrations that propagate through the soil into properties adjacent to the transit right of way (18). The transit designer should be aware of this potential as these vibration amplitudes

TABLE 2.—RANKING OF TRANSIT VEHICLE INTERIOR NOISE LEVELS FOR OPERATION IN SUBWAYS AT 30 MPH (4)

Cities (1)	Average sound pressure level, in decibels (2)
Philadelphia	98
Boston	95
New York	94
Chicago	92
Madrid (Talgo) ^a	92
Lisbon	91
London	87
Berlin	86
Paris (Rubber tire)	86
Stockholm	86
Washington (bus) ^b	85
Toronto	85
Hamburg	80

^a Measurements taken on at grade track.

^b Measurements taken on suburban expressway.

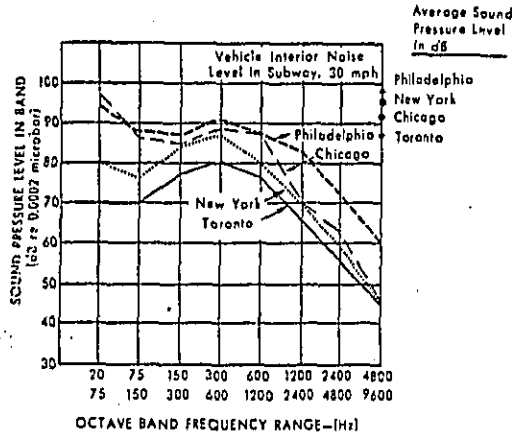


FIG. 3.—SOUND PRESSURE LEVEL-FREQUENCY DISTRIBUTION FOR TRANSIT VEHICLE INTERIOR NOISE (4)

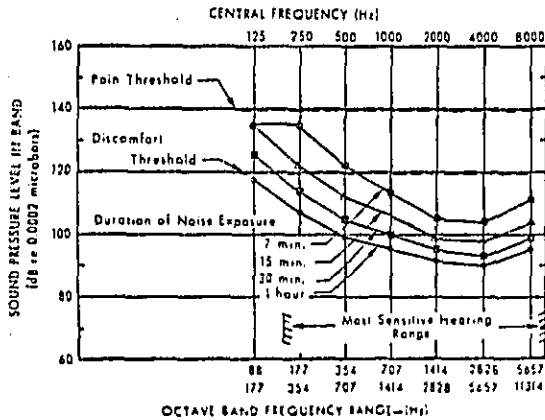


FIG. 4.—HUMAN SENSITIVITY AND SUGGESTED DAILY EXPOSURE LIMITS FOR NOISE (10)

may be sufficient to cause building components or household items to be set into annoying vibration.

NOISE LEVELS ASSOCIATED WITH EXISTING URBAN TRANSIT SYSTEMS

Information describing noise levels that are presently being generated in our existing transit systems suggests that these levels are high when com-

TABLE 3.—COMPARISON OF AVERAGE LOW FREQUENCY VIBRATION LEVELS RECORDED WITHIN TRANSIT VEHICLES (4)

System (1)	Average Vibration Level, in g		Average Frequency, in Hertz	
	Horizontal (2)	Vertical (3)	Horizontal (4)	Vertical (5)
Chicago	0.016	0.056	3.7	3.1
New York	0.034	0.031	4.0	4.8
Philadelphia	0.028	0.065	4.2	3.5
Toronto	0.028	0.025	5.0	5.0
London (40 mph)	0.032	0.123	5.1	3.1
Paris (rubber tire)	0.026	0.044	6.3	4.4
Paris (steel wheel)	0.027	0.089	5.7	4.4

TABLE 4.—NOISE LEVELS MEASURED IN SUBWAY STATIONS (4)

Systems (1)	Average Sound-Pressure Level, in decibels		
	Arrival (2)	Stop (3)	Departure (4)
Chicago	100	78	92
New York	100	75	98
Toronto	87	81	87
Berlin	94	73	88
Hamburg	97	78	88
Lisbon	105	88	104
Paris (rubber tire)	88	66	96
Paris (steel wheel)	99	77	96
Stockholm	96	82	93

pared to levels that are believed to be compatible with the urban environment. For example, noise levels in the interior of transit vehicles may approach 98 dBA. This is shown in Table 2 which lists noise levels measured in many different types of transit vehicles used throughout the world (4). Octave band frequency curves for three systems having the highest recorded noise levels are shown in Fig. 3. These curves, which give sound levels in limited frequency bands, describe the composition of noise as a function of frequency. The frequency spectrum is divided into nine octave bands which describe noise or vibration level in a way that makes it possible to determine in which portion

of the spectrum objectional noises are being developed so that appropriate noise control techniques can be applied.

In order to gain insight into the effect of the noise levels on transit riders, the measured sound pressure levels recorded in transit vehicles can be compared against Fig. 4 which shows human sensitivity to noise. It may be seen that the highest noise components are present in the frequency bands of 200 Hz to 800 Hz which is within the most sensitive range of the human ear. It may also be seen that these measured values are below maximum sound tolerance levels of 120 dB where actual discomfort is felt and 140 dB where pain is experienced by the listener (14).

Another measure of the effect of noise on the riding passenger may be made by comparing the noise within transit vehicles with noise levels that may cause damage or loss of hearing. Hearing damage risk levels for various daily ex-

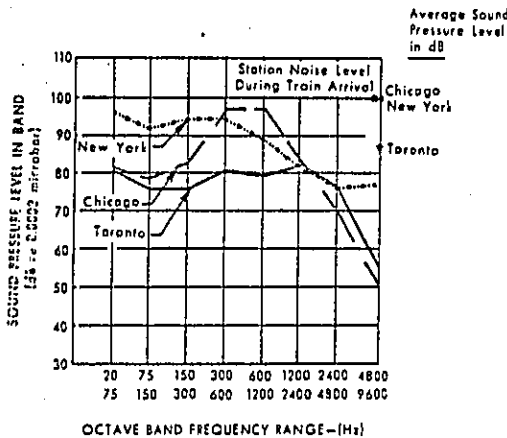


FIG. 5.—SOUND PRESSURE LEVEL-FREQUENCY DISTRIBUTION FOR STATION NOISE DURING TRAIN ARRIVAL (4)

posure times for periods of 10 yr or more have been suggested by the Committee on Hearing of the National Academy of Science and are also shown in Fig. 4 (10). It is clear from the Fig. that the lower the exposure time, the higher the noise level that can be tolerated. A comparison of Figs. 3 and 4 shows that for exposure times of less than 1 hr, which represents the maximum time that a passenger might be exposed to transit generated noise, the noise levels within vehicles are generally safe. However, these levels may be high enough to cause passenger annoyance that may result in decreased ridership and decreased community support of the transit system.

Vibration measurements in the interior of transit vehicles have been obtained by Davis and Zubkoff (4) and their low frequency data are summarized in Table 3. The evaluation of these data is difficult because there are no gen-

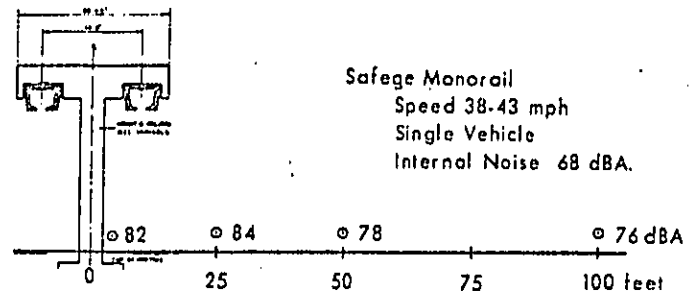
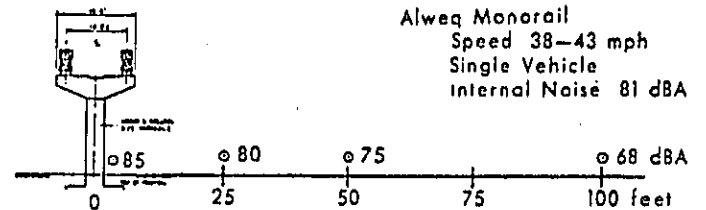
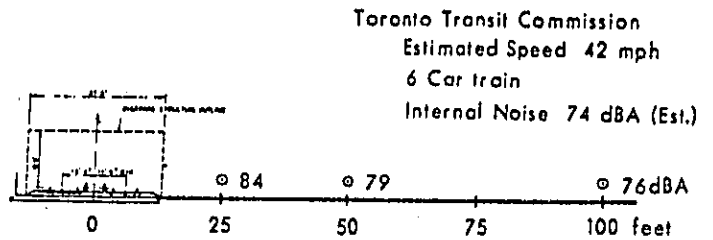


FIG. 6.—NOISE LEVELS RECORDED AT VARIOUS DISTANCES OUT FROM TRANSIT VEHICLES TRAVELING ON ELEVATED GUIDEWAYS AND AT GRADE (5)

erally accepted criteria for linking upper vibration limits and the subjective evaluation of what constitutes a comfortable ride (3). A simple comparison with the Meiser curves in Fig. 2, however, shows that these levels are in the range that is noticeable to individuals.

A comparison of noise levels in transit stations generated by vehicle operation has been presented by Davis and Zubkoff (4). The results of these measurements, shown in Table 4, indicate that the waiting passenger can in some cases be subjected to noise levels on the order of 100 dB with octave band frequency components as shown in Fig. 5. Such noise levels are generally higher than are presently thought acceptable for prolonged noise exposure.

The wayside community is exposed to airborne and structure-borne noise generated from transit vehicles travelling at grade and on elevated structures and from the ventilation facilities of subways. Lord, in the Manchester Study (5) has presented the results of noise measurements taken in open spaces adjacent to several monorail, conventional transit, and bus vehicles. The characteristics of these vehicles are compared in Table 5. Noise levels measured

TABLE 5.—PHYSICAL CHARACTERISTICS OF VARIOUS TRANSIT VEHICLE SYSTEMS

System	Characteristics				
	Length	Width	Empty weight, in pounds	Number of cars	Maximum speed, in miles per hour
(1)	(2)	(3)	(4)	(5)	(6)
Alweg Monorail	90 ft 3 in.	10 ft	50,000	single unit	50
Safege Monorail	57 ft	8 ft 2-1/2 in.	35,200	single unit	60
Conventional Rail Vehicle	69 ft 6 in.	9 ft 7 in.	50,400	8 car trains	60

4 ft above the ground surface at increasing distances out from these vehicles in open terrain are plotted in Fig. 6. These test data show that each of these relatively new systems produce external noise levels between 80 dBA and 86 dBA at a radial distance of 25 ft when travelling at about 40 mph at ground level in the open. The effect of vehicle speed may be taken into account by the fact that the noise level from all systems would be increased by about 3 dBA if the speed were increased to about 50 mph. It is useful to note from the data that the noise level from all systems falls off at between 4 dBA and 6 dBA per doubling of distance from the track (25 ft to 50 ft, 50 ft to 100 ft or 100 ft to 200 ft). Measurements also showed that an additional 2 dBA is produced by the elevated section of the Safege monorail system as compared with the ground level section. This increase can be attributed to increased track and support vibration which would be expected to be present on any elevated section using any vehicle system.

Wayside measurement of the noise levels generated by transit vehicles provides useful design information, but a word of caution must be inserted about the interpretation of these data. Noise levels generated from a source to a listener over a free field depend on a number of factors including atmo-

spheric conditions, ground topography, and season of the year. For example, people can perceive lower sound levels and are more sensitive to noise during the summer months when windows are normally open and when more time is spent out of doors. Therefore, wayside noise measurement programs should be carried out over a sufficiently long enough time period to ensure that a wide range of external factors are included in the data. The evaluation of these data then becomes a statistical problem and engineering judgment is required to properly develop appropriate design criteria.

NOISE LIMIT CRITERIA ON EXISTING TRANSIT SYSTEMS*

Several transit systems, operating conventional transit vehicles, have developed noise criteria based on assessments of passenger physiological dynamics and community acceptance. One of the most extensive and complete noise level criteria has been developed by the Toronto Transit Commission and is shown in Table 6 (1). Their basic overriding goal is that within the system the noise level should be low enough to permit a passenger to converse normally at a distance of approximately 3 ft. In acoustic terminology such a noise rating is based on a speed interference level (SIL) which recognizes that background noises can interfere with a person's ability to perceive sounds necessary for satisfactory speech intelligibility. It has been determined that speech perception is a function of the frequency of the background noise and for this reason the speech interference level is calculated by taking the arithmetic average of the sound pressure levels in the three octave bands centered around 500 Hz, 1,000 Hz and 2,000 Hz. In general, a SIL of 45 dB permits continuous conversation at a distance of about 10 ft, a SIL level of 55 dB permits speech in a normal voice at about 3 ft, while a SIL of 65 dB permits only strained and intermittent conversation to be maintained in a raised voice at a distance of 2 ft.

Noise control criteria based on the SIL covers the acceptability of noise in terms of speech communication but does not consider the entire audible range of the human ear which is most sensitive to sounds in the frequency range of from 20 Hz to 10,000 Hz. For this reason, speech may be possible in an otherwise fatiguing and annoying environment due to sound levels that occur in frequencies not considered in the SIL calculations. In order to avoid this problem and still maintain acceptable noise levels for speech communication, noise criteria curves have been developed (1). These curves, shown in Fig. 7, define maximum sound pressure levels in each of eight octave bands with an overall SIL rating value assigned to each particular noise criteria curve. Fig. 7 shows two different curves presently being used. The first set of curves, known as NC curves, are commonly used for specifying noise control in buildings while the second set, known as NCA curves, allow more noise in the low frequency octave bands and are reasonable to use when specifying noise control for the transportation environment.

In developing their noise level criteria, the TTC reasoned that a passenger will tolerate more noise while waiting for a transit vehicle than he will while riding; because the waiting passenger can in most cases see the approaching vehicle, feel the increasing air flow, and slowly become aware of the increasing noise level. Because of these conditions, a maximum noise level corresponding to the NCA 65 curve is suggested for station platforms. On the other hand,

TABLE 6.—TORONTO TRANSIT COMMISSION NOISE LEVEL CRITERIA (11)

Location (1)	Noise limit criteria (2)
General Overriding Criteria	Within the subway the noise level should be low enough to permit a passenger to converse normally at a distance of approximately 3 ft (Noise rating based on speech interference level, SIL).
Inside Subway Train	NCA 60 ^a
Station Platform	NCA 65 ^a
Adjacent Buildings	The expected noise and vibration levels for all buildings within 100 ft of the subway structure must be determined during the design stages so that noise and vibration criteria can be established for each building considering its usage and environmental conditions.

^a Intermittent short duration noise levels may reach NCA 70.

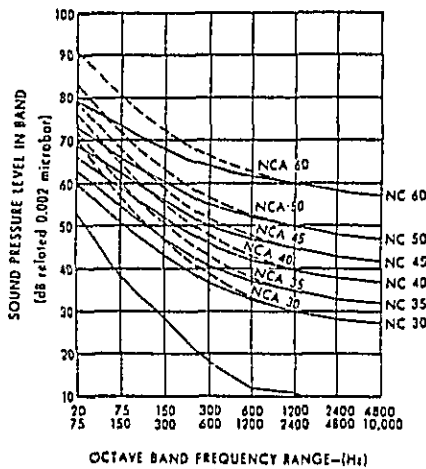


FIG. 7.—NOISE CRITERIA CURVES USED TO DEFINE PERMISSIBLE NOISE LEVELS (1)

the passenger riding in the transit vehicle expects to relax and his tolerance to noise is not as great as on the platform. Therefore inside trains a NCA 60 curve is suggested. With regard to the wayside community, no specific noise criteria levels were set because of diverse psychological factors involved and because of the variation in normal environment along the right of way. The expected noise and vibration levels for all buildings within 100 ft of the TTC subway facility are determined so that appropriate criteria can be established for each building considering its usage and environmental conditions.

More detailed noise control criteria for transit stations is available from the San Francisco BART system presently being completed (Table 7). The

TABLE 7.—SAN FRANCISCO BAY AREA RAPID TRANSIT NOISE LEVEL CRITERIA IN STATION AREAS

Station area (1)	Criteria and suggested treatment (2)
Open to street noise	Shield with kiosks and doors Unoccupied reverberation time less than 1 sec Cover 35 % of surface area (ceiling and walls) with sound absorbant material Reduce heel noise on floor surface
Adjacent to train (platform)	Sound level of NC40-NC50 to be maintained when no train is in station NC60 maximum level recommended when train is in the station or passing through the station at any speed
Interior public areas (all public areas except platform)	NC40 to NC50 level should be maintained in the absence of people Noise control techniques same as in "street noise" except for use of doors Vending or other equipment should not increase NC values for the space
Equipment rooms	Equipment noise should not raise NC levels in surrounding areas by more than 3 dB
Station agent booth	NC30 to NC40 level should be maintained when windows and doors are closed
Exterior areas	NC40 to NC45 levels measured at street level 25 ft from intake or outlet should not be exceeded for line vents and air exchange vents

BART criteria requires that on station platforms sound levels of NC40 to NC50 be maintained when no train is in the station and that NC60 is the maximum recommended level when a train is in the station or passing through the station at any speed. In other station areas stationary equipment or vending machines should not raise background noise levels above NC40 to NC50 levels.

Detailed suggestions for acceptable noise levels adjacent to transit systems are given in the Manchester Rapid Transit Study (5). It is suggested that wayside noise should not be any higher than the levels being generated by existing vehicle traffic. To put it more completely, maximum noise levels pro-

duced by a rapid transit vehicle for more than 10 % of the time in the peak period should not exceed the noise level which is already exceeded for 10 % of the time by existing traffic noise. Implementation of such a limit requires a knowledge of existing external noise levels such as those shown in Table 8 which forms the basis of the Manchester criteria. The most stringent limita-

TABLE 8.—MANCHESTER RAPID TRANSIT STUDY NOISE LEVEL CRITERIA IN AREAS ADJACENT TO RIGHT-OF-WAY (5)

Location (1)	Noise Level, in dBA	
	8 a.m.-6 p.m. (2)	1 a.m.-6 a.m. (3)
Arterial roads with many heavy vehicles and busses (at the curb)	68-80	50-70
Major roads with heavy traffic and busses; side roads within 45-60 ft of arterial or major roads	63-75	49-61
Main residential roads; side roads within 60-150 ft of heavy traffic routes, screened building courtyards	60-70	44-55
Residential roads with only local traffic	56-65	45-53

Note: Noise climato is the range of noise recorded for 80 % of the time. For 10 % of the time the level exceeds the higher level and for 10 % of the time it is less than the lower level.

Suggested Criteria: Maximum noise level produced by a transit vehicle for no more than 10 % of the time in the peak period should not exceed the noise level which is already exceeded for 10 % of the time by existing traffic noise.

TABLE 9.—PERMISSIBLE NOISE EXPOSURES PERMITTED BY WALSH-HEALEY ACT

Duration per day, in hours (1)	Sound level, in dBA (2)
8	90
6	92
4	95
3	97
2	100
1-1/2	102
1	105
1/2	110
1/4 or less	115

tion requires that transit vehicle night time operation generate noise levels below 45 dBA to 53 dBA at the location of residential roads carrying only local traffic. Higher levels of 56 dBA-65 dBA are permitted during the daytime hours and even higher levels are permitted near major traffic corridors.

Applicable federal noise and vibration legislation should be considered and

included when developing design criteria for new transportation systems. Particularly important are the Federal Occupational Noise Exposure provisions of the Walsh-Healey Act (12). This act states that protection against the effects of noise exposure shall be provided when the sound levels exceed those shown in Table 9, when measured on the A scale of a standard noise sound level meter. When noise levels are determined by octave band analysis, an equivalent A-weighted sound level may be determined by noting the sound level corresponding to the point of highest penetration into the sound level contours prescribed in the act.

State and local noise ordinances are becoming common and should be considered whenever they apply. For instance, the California Vehicle Code has provisions that prescribe vehicle noise limits. New York and Chicago are examples of major cities that have enacted rather strict noise limiting ordinances in the last few years; their lead can be expected to be followed by other cities in the future.

DESIGN METHODS TO LIMIT NOISE AND VIBRATION, p 907

It is useful for the designer to remember that noise and vibration control can be achieved most effectively by quieting the noisiest components first. In transit systems, tests have shown that the wheel and the guideway are the major noise and vibration sources followed in order by the propulsion system, auxiliary car carried equipment (compressors, generators and pumps), and fixed plant equipment (electrical substations, ticket and vending equipment, and ventilation equipment). A detailed description of these major noise sources along with details of the common exciting sources and the noise radiating areas concerned are ranked in Table 10 (17).

Wheel-guideway interaction is the major source of noise and vibration but proper design as well as follow up maintenance programs can minimize their effect on ride comfort. In steel-wheel systems, proper guideway alignment, rail grinding and wheel grinding are necessary if required comfort levels are to be met. In addition, maintenance programs that maintain these system components within suitable limits will help to maintain system ride comfort and minimize community intrusion.

Rubber-tire transit systems also require proper design and adequate maintenance programs if they are to operate at low noise levels. A common belief that is often heard, states that rubber tired transportation systems are naturally quieter than steel-wheel steel-rail systems. However, there are no published data to support this claim (4). Tires are noisy, because when a section of tire comes into contact with the guideway, it is compressed by the weight of the vehicle which causes a reduction in the volume of the tire grooves which forces out air under pressure. This air movement, along with the re-entry of air back into the tread as it is unloaded, creates the characteristic tire sound. A smoother tread could be used to eliminate this noise, but such a tire would not provide safe braking under wet weather conditions. Thus transit tire design becomes a compromise between safety and quietness.

Tire rumble can also be a problem particularly on rough guideways. Rumble is caused by the vibration of the tire casing when it strikes an irregularity in the guideway surface. Construction of smooth guideways and proper maintenance programs can reduce noise and vibration from this source.

Transit guideway placement (elevated, at grade or in tunnels) and roadbed

design can also effect the magnitude of generated noise and vibration. For instance, underground transit operation is probably the most critical condition for the generation of noise in the interior of transit vehicles (13,19). Measurements have shown that noise levels are about 6 dBA lower in the same vehicle when running on open track than when running in a tunnel. There also seems to be a 6-dBA decrease in interior noise level for vehicles in tunnels travelling over tie and ballast track bed versus operation over a concrete track bed, (0). It would appear from the aforementioned that guideway selection is an important design characteristic for the transit designer who is concerned with limiting noise and vibration.

The application of good industrial design standards can be very effective in reducing noise and vibration from car carried and fixed equipment. As an example, noisy motors can be silenced with only a little redesign of the cooling fans. Similarly the reduction of tip speed and aerodynamic redesign of the cooling fans of air conditioning systems can significantly reduce the noise

TABLE 10.--MAJOR RAPID TRANSIT NOISE SOURCES (17)

Component (1)	Excitation (2)	Radiator (3)
(a) Major—wheel and guideway		
Wheel	Stick-slip of steel wheel to rail. Tire tread of rubber tires.	Sides of wheel
Steel Guideway Concrete Guideway Switches, cross-overs	Stick-slip of wheel to rail. Surface roughness. Discontinuity of guideway.	Sides of rail Roadbed Wheels, roadbed, rail
(b) Moderate—propulsion system		
Propulsion	Unbalance; gear and bearing irregularity; magnetostriktion.	Motor, car body, gear box
Power Collection	Friction on conductor.	Shoes, attached parts
Brake	Stick-slip.	Shoe, break disk or wheel tread, air exhaust
Elevated Structure	Wheel-guideway irregularities.	Girders, roadbed, columns
(c) Possibly important ^a —auxiliary equipment		
Rolling Gear and Car body	Car vibration, rattles, couplers.	Large car body surfaces, doors, gates, couplings
Vehicle equipment	Blade turbulence from fans, unbalance	Air stream, vehicle roof
Stationary equipment	Blade turbulence from fans, unbalance, pump noise.	Structure, air exhaust
Wind noise	Boundary layer turbulence.	Air stream

^a Reasonable industrial design standards and proper maintenance should limit noise generation from this class of sources.

from these components. Such treatment of standard equipment, when required as a performance specification when the system is first ordered, will add little to the original cost but will lower noise and vibration levels significantly.

CONCLUSIONS

In order to develop an improved understanding of the most important factors that contribute to passenger comfort in rapid transit systems, the preceding pages have presented information on transit generated noise and vibration. Knowledge of existing urban noise levels may be used as a measure against which to compare transit generated noise levels. Information on limiting values of noise and vibration that have been adopted by the major transit operators provide a useful guide to the wide range of possible forms that any criteria can take as well as specific information on limiting values.

It is useful to remember however, that many of the new transit systems that are being proposed have much different operating characteristics than even a single conventional rail rapid transit car. For example, new vehicles may be smaller and lighter than conventional rapid transit cars and thus would naturally be expected to generate lower noise levels. On the other hand, the small size and compactness of these vehicles will be used to advantage by designers who will be able to weave transportation corridors into tight urban centers and even into and through major structures. Thus effective controls over noise and vibration levels should not be neglected.

Past experience has indicated that certain components of any transit system will contribute the major share of noise and vibration. Particular care should be taken to quiet the wheel and the guideway as well as the propulsion system. The application of standard industrial methods should effectively silence other system components such as air conditioning, pumps, and control equipment to acceptable levels.

The transportation designer and engineer should bear in mind that noise and vibration control is best carried out early in the design stage of any transit project. This can avoid costly and sometimes ineffective remedial noise and vibration control measures that may be required to quiet a noisy system that is already in operation.

ACKNOWLEDGMENTS

This report was produced as part of a program of Research and Training in Urban Transportation sponsored by the Urban Mass Transportation Administration of the U.S. Department of Transportation and this support is gratefully acknowledged.

The results and views expressed are the independent products of university research and are not necessarily concurred in by the Urban Mass Transportation Administration of the Department of Transportation.

APPENDIX.—REFERENCES, p. 907-908

1. Beranek, L. L., *Noise Reduction*, McGraw-Hill Book Co., Inc., New York, 1960.

2. Bugliarello, G. B., ed. *Noise Pollution*, Biotechnology Program, Carnegie Mellon University, Pittsburgh, Pa., Feb., 1968.
3. Cooperrider, N. K., "Secondary Suspension Requirements for Tracked Vehicles," *High Speed Ground Transportation Journal*, Vol. 111, No. 2, May, 1969, pp. 255-267.
4. Davis, E. W., and Zubkoff, W. J., "Comparison of Noise and Vibration Levels in Rapid Transit Vehicle Systems," *Technical Report 216*, prepared for the National Capitol Transportation Agency by Operations Research, Inc., Silver Springs, Md., 1964.
5. DeLeuw, Cather and Partners, *Manchester Rapid Transit Study*, Prepared for the City of Manchester, England, Vol. 1-2, Aug., 1967.
6. Gierke, H. E. von, "Biodynamic Response of the Human Body," *Applied Mechanics Reviews*, Vol. 17, Dec., 1964, pp. 951-958.
7. Goldman, E. E. and Gierke, H. E. von, "Effects of Shock and Vibration on Man," *Shock and Vibration Handbook*, C. M. Harris and C. S. Crede, ed., McGraw-Hill Book Co., New York, Vol. 3, Chap. 44, 1961.
8. Gulgnard, J. C., "Effects of Vibration on Man," *Journal of Environmental Sciences*, Aug., 1966, pp. 29-32.
9. Harris, C. M. and Aitken, B. H., "Noise in Subway Cars," *Noise and Vibration*, Feb., 1971, pp. 12-14.
10. Kryter, K. D., Ward, W. D., Miller, J. D. and Eldredge, D. H., "Hazardous Exposure to Intermittent and Steady-State Noise," *Journal of the Acoustical Society of America*, Vol. 39, No. 3, Mar., 1966, pp. 451-464.
11. Murray, R. J., "Noise and Vibration Theories," *Report No. 107*, Subway Construction Branch, Toronto Transit Commission, Toronto, Canada, May, 1967.
12. "Occupational Noise Exposure," Walsh-Healey Act, *Federal Register*, Vol. 34, No. 96, Tuesday, May, 20, 1969 (As revised from the Federal Register, Saturday, Jan., 24, 1970).
13. Parsons Brinckerhoff, Tudor, and Bechtel, "Acoustic Studies," *Report No. 8*, Prepared for the San Francisco Bay Area Rapid Transit District, June, 1968, p. 157.
14. Peterson, A. P., and Gross, E. E., *Handbook of Noise Measurement*, 6th. Edition, General Radio Company, West Concord, Mass., 1967, p. 282.
15. Reither, H. J. and Meister, F. J., "Human Sensitivity to Vibration," *Forschung auf dem Gebiete des Ingenieurwesens*, Vol. 2, No. 11, 1931, pp. 381-386. (Translation Report F-TS-616-RE, Wright Field, 1946).
16. Richard, F. E. Jr., Hall, J. R. Jr., and Woods, R. D., *Vibrations of Soils and Foundations*, Prentice-Hall Inc., Englewood Cliffs, N.J., 1970, p. 414.
17. Salmon, V. and Olsson, S. K., "Noise Control in the Bay Area Rapid Transit System," Report Prepared for Parsons Brinckerhoff, Tudor and Bechtel by the Stanford Research Institute, Menlo Park, N.J., Feb., 1965, p. 109.
18. Silver, M. L., and Belytschko, T., "Transit Induced Vibration in Structures Adjacent to the Right of Way," Progress Report to the Urban Mass Transport Administration, Department of Materials Engineering, University of Illinois at Chicago Circle, Sept., 1971.
19. Wilson, P. W., "Rapid Transit Noise and Vibration," Presented at the Rail Transit Conference of the American Transit Association, Apr., 1971, p. 26.
20. Wilson Committee, "Noise," *Final Report*, Her Majesties Stationary Office, Communication 2056, 1963.

TRANSPORTATION ENGINEERING JOURNAL

Proceedings of the American Society of Civil Engineers

FEDERAL RESEARCH IN URBAN TRAFFIC CONTROL¹

By Juri Raus¹ and Philip J. Tarnoff²

(Reviewed by the Urban Transportation Division)

INTRODUCTION

In May, 1968, the Federal Highway Administration initiated a major emphasis research project titled Urban Traffic Control System (UTCS). It began with a study of system requirements and the development of specifications for a digital computer controlled traffic signal system in Washington, D.C. to be used as a real world street laboratory to test new and advanced traffic control techniques and programs.

The facility was later expanded to include a Bus Priority System (BPS) to meet the requirement initiated by the Urban Mass Transportation Administration of the Department of Transportation. BPS is a joint program with the Federal Highway Administration and UMTA. The Bus Priority System will be used to experimentally determine if bus delays can be decreased by giving buses preferential treatment at signalized intersections. This system configuration parallels that of the Urban Traffic Control System, so both systems have been combined into a single laboratory for testing advanced urban traffic control techniques and strategies.

Note.—Discussion open until April 1, 1973. To extend the closing date one month, a written request must be filed with the Editor of Technical Publications, ASCE. This paper is part of the copyrighted Transportation Engineering Journal of ASCE, Proceedings of the American Society of Civil Engineers, Vol. 98, No. TE4, November, 1972. Manuscript was submitted for review for possible publication on September 17, 1971.

¹Presented at July 26-30, 1971, ASCE National Transportation Engineering Meeting, held at Seattle, Wash.

²Highway Research Engr., Proj. Manager, Traffic Systems Div., Off. of Research, U.S. Dept. of Trans., Fed. Highway Adm., Wash., D.C.

³Gen. Research Engr., Traffic Systems Div., Off. of Research, U.S. Dept. of Trans., Fed. Highway Adm., Wash., D.C.

VOL.98 NO. TE4, NOV. 1972

TRANSPORTATION ENGINEERING JOURNAL OF ASCE

PROCEEDINGS OF
THE AMERICAN SOCIETY
OF CIVIL ENGINEERS



PIPELINE
HIGHWAY
AIR TRANSPORT
URBAN TRANSPORTATION
AEROSPACE

also includes papers from
WATERWAYS, HARBORS AND COASTAL
ENGINEERING DIVISION

© American Society
of Civil Engineers
1972

AMERICAN SOCIETY OF CIVIL ENGINEERS

BOARD OF DIRECTION

President
John E. Rinne

President-elect
Charles W. Yodar

Past President
Oscar S. Bray

Vice Presidents
John W. Frazier
James L. Konski

Directors
William C. Ackermann
B. Austin Barry
Walter E. Blassey
Bevan W. Brown, Jr.
L. LeRoy Crandall
Elwood D. Dobbs
Lloyd C. Fowler
William R. Gibbs
Paul C. Hessler, Jr.
Hugh W. Hempel
Christopher G. Tyson

Dean F. Peterson
L. A. Woodman

Elmer B. Isaak
Russel C. Jones
Thomas C. Kavanagh
Frederick R. Knoop, Jr.
Arno T. Lenz
Oscar T. Lyon, Jr.
John E. McCall
Jack McMinn
John T. Merrifield
Cranston R. Rogers

EXECUTIVE OFFICERS

Eugene Zworyk, *Executive Director*
Don P. Reynolds, *Assistant Executive Director*
Joseph McCabo, *Director—Education Services*
Edmund H. Lang, *Director—Professional Ser-
vices*

William N. Carey, *Secretary Emeritus*
William H. Wisely, *Executive Director Emeritus*
William S. LaLonde, Jr., *Treasurer*
Elmer K. Timby, *Assistant Treasurer*

COMMITTEE ON PUBLICATIONS

Walter E. Blassey
Elwood D. Dobbs

Arno T. Lenz
John E. McCall

Technical Publications
Richard R. Torrens, *Editor*
Robert D. Walker, *Associate Editor*
Geraldino Cioffi, *Assistant Editor*
Elsino C. Cuddihy, *Editorial Assistant*
Virginia G. Fairweather, *Editorial Assistant*
Victoria Koestler, *Editorial Assistant*
Frank J. Loeffler, *Draftsman*

Information Services
Irving Amron, *Editor*

PARTICIPATING GROUPS

AIR TRANSPORT DIVISION

Executive Committee
John M. Duggan, *Chairman*
Edwin R. Brohan, *Vice Chairman*
Andy M. Attar, *Secretary*
Phillip P. Brown
Frederick R. Knoop, Jr., *Board Contact Member*

Johannes W. Kurz
B. M. Singer

Publications Committee
H. K. Friedland, *Chairman*
Everett Carter
F. J. Wegman
Andy M. Attar, *Exec. Comm. Contact Member*

HIGHWAY DIVISION

Executive Committee
William B. Drake, *Chairman*
John J. Walsh, *Vice Chairman*
Jose J. Cortes, *Secretary*
Fred J. Benson
Oscar T. Lyon, Jr., *Board Contact Member*

Lloyd G. Byrd

Publications Committee
Donald L. Woods, *Chairman*
John L. Boulton
John A. Deisinger
Dennis J. Fitzgerald
John E. Huffman
Ronald W. Hudson
R. A. Jiminez
Lloyd G. Byrd, *Exec. Comm. Contact Member*

R. E. Johnson
J. A. Leadabrand
Roger V. LeClere
Russell M. Lewis
Bob L. Smith
Wm. A. Yijanson

TECHNICAL COUNCIL ON AEROSPACE

Executive Committee
Stewart H. Johnson, *Chairman*
J. Frank Burke, *Vice Chairman*
William D. Esser, *Secretary*
J. S. Dutton
Robert E. Blawie, *Board Contact Member*

James G. Winter

PIPELINE DIVISION

Executive Committee
Raymond C. Regnier, Jr., *Chairman*
William F. Quinn, *Vice Chairman*
Melville S. Priest, *Secretary*
Ralph C. Hughes, Jr.
Lloyd C. Fowler, *Board Contact Member*

Henderson E. McGeo

Publications Committee
George C. Govatos, *Chairman*
Gary W. Edwards
John A. Haydon
Melville S. Priest, *Exec. Comm. Contact Member*

Richard D. Howard
Iraj Zandit

URBAN TRANSPORTATION DIVISION

Executive Committee
Reginald J. Sutherland, *Chairman*
Nilson Pikarsky, *Vice Chairman*
Edward F. Sullivan, *Secretary*
Edward S. Olcott

Francis C. Turner
James R. McBreon
Carl Selinger

Publications Committee
Salvatore J. Ballomo, *Chairman*
Donald L. Garrett
Joseph W. Guyton
Edward F. Sullivan, *Exec. Committee Contact Member*

CONTENTS

Papers	Page
URBAN ROAD PRICING THROUGH SELECTIVE PARKING TAXES by Robert E. Burns (Urban Transportation Division)	739
EVALUATION OF NEW SYSTEMS FOR URBAN TRANSPORTATION by Reed H. Winslow and Jerry L. Pfeffer (Urban Transportation Division)	757
MANAGEMENT SYSTEM FOR CAMPUS TRAFFIC PLANNING by Michael J. Quillen and Jason C. Yu (Urban Transportation Division)	769
TRANSPORTATION AND RETIREMENT by Frances M. Carp (Urban Transportation Division)	787
TIME STABILITY OF ZONAL TRIP PRODUCTION MODELS by Norman Ashford and Frank M. Holloway (Urban Transportation Division)	799
DEMAND ACTIVATED TRANSPORTATION FOR THE ELDERLY by Charles B. Nottess and Robert E. Paaswell (Urban Transportation Division)	807

(over)

This Journal is published quarterly by the American Society of Civil Engineers. Publications office is at 345 East 47th Street, New York, N.Y. 10017. Address all ASCE correspondence to the Editorial and General Offices at 345 East 47th Street, New York, N.Y. 10017. Allow six weeks for change of address to become effective. Subscription price is \$8.00 per year with discounts to members and libraries. Second-class postage paid at New York, N.Y. and at additional mailing offices, T.E.

The Society is not responsible for any statement made or opinion expressed in its publications.

	Page		Page
COMMUNITY VALUES IN TRANSPORT NETWORK EVALUATION by Dan G. Haney and George E. Klein (Urban Transportation Division)	823	TRENDS IN OFFSHORE AIRPORTS by Richard D. Harza (Air Transport Division)	985
CEMENT MORTAR LINING OF 20-FT DIAMETER STEEL PIPE by James E. Wolfe (Pipeline Division)	837	DYNAMIC RESPONSE OF MODEL PAVEMENT STRUCTURE by Stephen F. Brown and David I. Bush (Highway Division)	1005
MICHIGAN TRANSPORTATION IN THE SEVENTIES by William C. Taylor (Urban Transportation Division)	847	EXPRESSWAY RAPID TRANSIT by George Krambles (Urban Transportation Division)	1023
TRANSPORTATION RESEARCH FOR COMMUNITY OBJECTIVES by Arthur Saltzman, Alice E. Kidder, Florentine V. Sowell, and Sidney H. Evans (Urban Transportation Division)	855	SYSTEMATIC STRESS ANALYSIS OF CIRCULAR PIPE by Junkichi Katoh (Pipeline Division)	1039
STATISTICAL DECISION IN FORECASTING PLANNING DATA by Kumares C. Sinha (Urban Transportation Division)	865	<hr/> DISCUSSION Proc. Paper 9309 <hr/>	
LOCAL RURAL ROAD COSTS AND ECONOMIES OF SCALE by William D. Berg (Highway Division)	881	PLANNING FOR CAMPUS TRAFFIC AND PARKING, by Joseph W. Guyton and George L. Reed (Feb., 1971. Prior Discussions: Nov., 1971, Feb., 1972). closure	1067
NOISE AND VIBRATION CONTROL IN NEW RAPID TRANSIT by Marshall L. Silver (Urban Transportation Division)	891	INITIAL ECONOMIC EVALUATION OF SLURRY PIPELINE SYS- TEMS, by Edward J. Wasp, Terry L. Thompson and Thomas C. Aude (May, 1971. Prior Discussion: Feb., 1972). closure	1068
FEDERAL RESEARCH IN URBAN TRAFFIC CONTROL by Juri Raus and Phillip J. Tarnoff (Urban Transportation Division)	909	PLANNING'S ROLE IN STANDARDS FOR FUTURE HIGHWAYS, by Ralph D. Brown, Jr. (May, 1971. Prior Discussion: Feb., 1972). errata	1068
CURRENT METHODS FOR IMPROVED TIRE-PAVEMENT INTERACTION by Bob M. Gallaway and Jon A. Epps (Highway Division)	915	NEW HIGHWAY BRIDGE DIMENSIONS FOR SAFETY, by John N. Clary (May, 1971. Prior Discussion: Feb., 1972). closure	1070
KEYED JOINT PERFORMANCE UNDER HEAVY LOAD AIRCRAFT by John L. Rice (Air Transport Division)	931	ESTIMATION OF DESIGN FREEZING INDICES, by George McCormick (Aug., 1971. Prior Discussion: May, 1972). closure	1070
CURBSIDE SERVICE SUBWAYS by Charles J. Swet (Urban Transportation Division)	941	SIMULATION OF WATERWAY TRANSPORT SYSTEMS, by Joseph L. Carroll and Michael S. Bronzini (Aug., 1971. Prior Discussions: Feb., May, 1972). closure	1071
SATELLITE TRANSIT AT SEATTLE-TACOMA AIRPORT by Ralph Mason (Air Transport Division)	953	TRANSPORTATION RESEARCH NEEDS IN CIVIL ENGINEERING, by Robert F. Baker (Aug., 1971. Prior Discussion: Feb., 1972). closure	1072
CONSIDERATIONS OF TENSION TIE PROBLEMS by Lloyd C. Fowler, Richard P. Lundahl, and Robert W. Purdie (Pipeline Division)	969		

140
What Should Be the Noise Limit on Railway ?

RECEIVED

FEB 5 1972

NOISE ABATEMENT PROGRAM
INFORMATICS INC.

Tadamoto Nimura and Toshio Sone
(Department of Electrical Engineering,
Tohoku University)

WS
1/2
PT (1)

What level should be defined as the limit on a rapid transit train noise is suggested through many-sided discussions, namely at first through the survey of community response to train noise (described in another paper submitted), secondly through comparison with aircraft noise, in the third place through reference to motor carrier noise environment standards and through considerations on techniques for train noise control.

As to the last subject, a functional flow logic diagram for train/railroad noise system is prepared. Various approaches for train noise reduction are discussed on the basis of the diagram, and a noise limit in the near future is proposed from the present technical level and the economical point of view.

The Public Nuisance Abatement Council of Sendai city came to the following conclusions under authors' leadership in the beginning of the construction work of the New Tohoku Line, which will be opened to traffic in 1976;

(1) Peak level of train noise along the New Tohoku Line should be 70 dB(A) or less in the dwelling area. This demand should be met as early as possible (within 2 or 3 years after the opening to traffic).

(2) At the time of opening to traffic it should be 75 dB(A) or less in daytime and 70 dB(A) or less in night time.

730435

(3) A vibration propagated from the railroad tracks should not give any trouble to residents and houses in the dwelling area.

(4) A special regard should be paid to the establishments such as a hospital, a school and others, for which quiet is indispensably necessary.

(5) If the above value were judged unattainable, the land utilization plan including purchase of a lot, the decrease of the speed, an underground railway and other steps should be taken into consideration.

(6) If the residences exposed to a train noise above 70 dB(A) still exist after the practice of the above steps, the soundproofing, moving into another house and other compensations should be made.

(7) Laws and institutions necessary for practice of these steps should be provided as early as possible.

(8) As to the work for maintenance of railroad the reduction of the noise should be contrived through the improvement of operations and such.

(9) Sufficient regard should be paid on noise due to the construction work.

The reasons why we came to these conclusions will be reported in detail.

12408

DEC 12 1973

ACUSTICA

S. HIRZEL VERLAG · STUTTGART

Vol. 28

1973

Heft 6

Prediction of Rail-Wheel Noise from High Speed Trains

by S. PETERS

RECEIVED

NOV 20 1973

NOISE ABATEMENT PROGRAM
INFORMATICS INC.

Prediction of Rail-Wheel Noise from High Speed Trains

by S. PETERS*

Research Department, Railway Technical Centre, Derby

Summary

The noise radiated by high speed railway trains is generated predominantly by the vibration of the rails and the wheels and a close relationship has been observed experimentally between vehicle speed and rail-wheel noise levels measured on the dBA scale. This relationship has been incorporated in a simple acoustic model of a train and the model used to predict the peak noise levels experienced during the passage of conventional British Railway stock. The predictions have shown a 95% probability of being within 5 dB of observed results; the predictive method is to be used as part of a larger model for the prediction of community noise reaction.

Vorausbestimmung des Schiene-Rad-Lärms bei Hochgeschwindigkeitsbahnen

Zusammenfassung

Der von Hochgeschwindigkeitsbahnen abgestrahlte Lärm wird vorwiegend durch Schwingungen der Schienen und Räder hervorgerufen. Es wurde experimentell beobachtet, daß zwischen der Fahrzeuggeschwindigkeit und den A-bewerteten Schiene-Rad-Geräuschpegeln eine enge Beziehung besteht. Diese Beziehung wurde auf ein einfaches akustisches Modell einer Schienenbahn übertragen, das zur Vorausbestimmung der Lärm Spitzenpegel dient, die bei der Vorbeifahrt eines konventionellen British Railway Zuges zu erwarten sind. Die Voraussagen stimmen mit einer Sicherheit von 95% auf 5 dB genau mit den beobachteten Werten überein.

Die Vorausbestimmungsmethode soll als Bestandteil eines umfassenderen Modells zur Vorausberechnung der Einwirkung von Umweltlärm verwendet werden.

Prédiction du bruit des rails et des roues de trains à grande vitesse

Sommaire

Le bruit produit par les trains à grande vitesse provient d'une façon prédominante de la vibration des rails et des roues, et on a observé expérimentalement une relation étroite entre la vitesse du train et les bruits rails-roues, les niveaux étant mesurés sur l'échelle dBA. Cette relation a été introduite dans un modèle acoustique simple de train et le modèle a été utilisé pour produire les niveaux des pointes de bruit faisant l'objet d'expériences pendant le passage d'un train normal du British Railways. Les niveaux prévus ont une probabilité de 95% d'être à moins de 5 dB des résultats observés; la méthode de prédiction sera utilisée comme une partie d'un modèle plus important pour la prédiction de la réaction de la population au bruit.

1. Introduction

The noise generated by high speed railway trains is generated predominantly by the vibration of the rails and wheels and a close relationship has been observed between vehicle speed and rail-wheel noise levels measured on the dBA scale. This work is inspired by the increasing demand for predictions of the impact of new patterns of railway usage on the acoustic environment.

At less than 20 m from a diesel powered train the peak noise level can be associated with the passing locomotive rather than with rail-wheel noise. At distances greater than 20 m rail-wheel noise is predominant. Locomotive noise is a function of engine

speed and cooling fan speed but as in the majority of B.R. locomotives the diesel drives an electric alternator the engine speed is indirectly related to the locomotive speed. Consequently there is poor correlation between locomotive speed and locomotive noise level. The highest engine noise levels are measured when the power demand is greatest. This would be during hill climbing or whilst accelerating. The prediction of locomotive noise at any site is difficult and requires a knowledge of the manner in which the locomotive is to be operated, the locomotive type and noise characteristic and the local and regional gradients and curves. The prediction of rail-wheel noise levels is somewhat easier and for conventional rolling stock levels are strongly correlated with the train make up, the train velocity and the distance between the observation point and the track.

* Lecture given at Second Anglo/Spanish/Netherlands Symposium on Environmental Acoustics, London, July 1972.

A simple predictive theory for rail-wheel noise levels has been derived and in the summer of 1971 a series of measurements were made from which the velocity dependence of the noise was determined together with an indication of the likely accuracy of a predicted noise level.

2. Experimental work

Measurements were conducted at Thirsk in the North Riding of Yorkshire, England, alongside the main York-Darlington railway line. The site that was chosen had a number of favourable characteristics. On both sides of the track the land was flat and clear of obstructions to a distance of about 800 m. The track was straight and level for some distance on either side of the site and high speed running was possible. A wide variety of train speeds and traffic types could be expected. Measurements were performed with microphones 1.5 m above ground level, corresponding to 0.5 m above rail-head level. Seven measuring positions were located on each side of the track at distances from the track of up to 400 m. All microphones, associated amplifiers and tape recorders were regularly calibrated with piston-phones.

A total of 64 useful records of 39 trains were obtained during 13 hours of recording spread over 2 days. Throughout the experiment a 2.5 m/s wind blew diagonally across the track. A typical record is shown in Fig. 1.

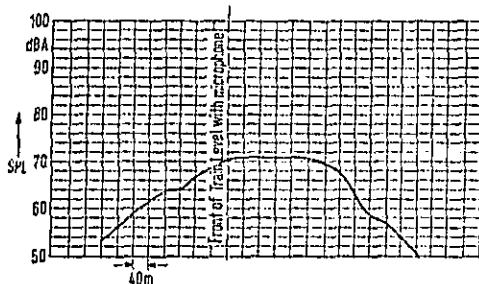


Fig. 1. Typical trace of A-weighted sound pressure level (SPL).
Train speed: 152 km/h,
Train type: Down passenger, class 45 locomotive and eight coaches,
Microphone position: 200 m from track, eastern side,
Peak level: 71 dBA.

3. Simple theory and analysis of experimental results

The mean square sound pressure \bar{p}^2 at any point along the perpendicular bisector of a finite line

source in free space is given by:

$$\bar{p}^2 = \frac{l \rho c}{2 \pi y} \tan^{-1} \frac{l}{2y}$$

where l = source length,
 y = distance from the observer to the line source,
 l = source intensity per unit length,
 ρc = characteristic impedance of air.

Expressions of this type may be obtained by integrating the sound radiation from a linear array of discrete spherical sources.

For the case with which we are concerned the line source is not in free space but in a half space bounded by the ground. The observed \bar{p}^2 averaged over a frequency band that is wide enough to include a large number of radiating modes is approximately:

$$\bar{p}^2 \approx \frac{l \rho c}{\pi y} \tan^{-1} \frac{l}{2y} \quad (1)$$

If each wheel of a train and associated short segment of rail is regarded as a simple source, then eq. (1) may be used to represent the sound radiation from the whole train.

Let $D = y/l$ (l is now train length),
 N = number of identical vehicles,
 A = number of axles per vehicle,
 l_v = vehicle length,
 W = rail-wheel noise source strength,

then the mean square pressure may be written

$$\bar{p}^2 = \frac{A \rho c W}{\pi D l_v^2 N} \tan^{-1} \frac{l}{2D} \quad (2)$$

Consequently the Sound Pressure Level (SPL) re $20 \mu\text{N/m}^2$ can be derived:

$$SPL = 10 \log \frac{W}{10^{-12}} + 10 \log \left(\frac{1}{D} \tan^{-1} \frac{l}{2D} \right) - 20 \log l_v + 10 \log \frac{A}{N} - 5 \text{ dB} \quad (3)$$

where W has units of watts and l_v has units of meters. Current standard coaches (e.g. B.R. Mk. 11 series) are 20 m long and have four axles. Eq. (3) is usefully rewritten as:

$$SPL = 10 \log \frac{W}{10^{-12}} + 10 \log \left(\frac{1}{D} \tan^{-1} \frac{l}{2D} \right) - 20 \log \frac{l_v}{20} + 10 \log \frac{A}{4N} - 25 \text{ dB} \quad (4)$$

In this equation the peak SPL observed as a train of identical vehicles passes some point is expressed as a function of the rail-wheel source power (W), the ratio of the observer to track distance to the train

length (D), the length of each vehicle (l_v) and the number of vehicles and the number of axes per vehicle (the train make up, $A/(4N)$). The function $10 \log \left(\frac{1}{D} \tan^{-1} \frac{1}{2D} \right)$ has been tabulated and all measured peak levels were adjusted so that they represented effective values of peak noise level at a distance of one train length away from the track; corrections were supplied for train make up using the term $10 \log(A/4N)$ whereby the peak levels were reduced to the equivalent level of a single four axle vehicle. A vehicle length correction was applied so that the effective vehicle length was 20 m.

Results from each side of the track were plotted as a function of velocity and these are shown in Figs. 2 and 3. It was immediately apparent that the

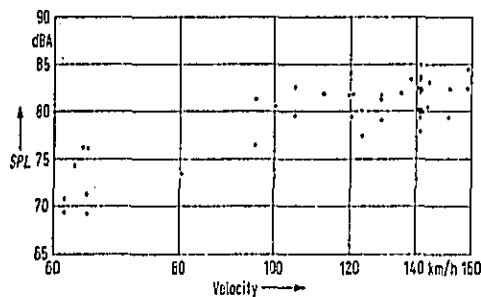


Fig. 2. Peak A-weighted sound pressure level (SPL) corrected for train make-up and reduced to a distance of 1 train-length, east (downwind).

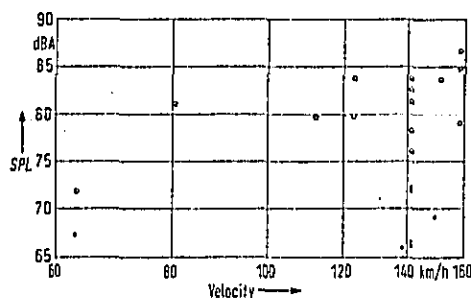


Fig. 3. Peak A-weighted sound pressure level (SPL) corrected for train make-up and reduced to a distance of 1 train-length, west (upwind).
 ○○○ Measuring positions up to 50 m from track,
 ●●● measuring positions more than 50 m from track.

levels of upwind results at more than 50 m from the track were much less than those of the bulk of our measurements. The low results probably represent measurements taken in the upwind acoustic shadow

(BERANEK [1]) and these results were not used in any subsequent calculation. At this stage in the analysis it was suspected that there might be some further distinction between the measurements on the two sides of the track and regression lines were calculated for each group of data. These are shown in Fig. 4. In the middle of the speed range, about

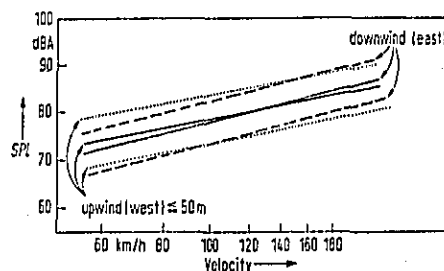


Fig. 4. Regression of corrected peak A-weighted sound pressure levels on velocity with error bounds of two standard errors of estimate on either side of regression lines.

80 km/h to 160 km/h, the difference between the two regression lines is small compared to the error bounds which are being considered; beyond this range the difference is significant and reflects the requirement for more work of both an empirical and theoretical nature. Nevertheless the downwind and near up-wind results were pooled and a new regression line calculated. This regression line is shown in Fig. 5 and is embodied in the following equation:

$$10 \log \frac{W_1}{W_2} = 25 \log \frac{V_1}{V_2} \pm 5 \text{ dB.} \quad (5)$$

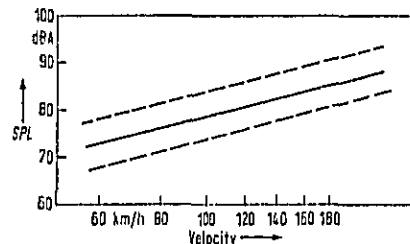


Fig. 5. Regression of corrected peak A-weighted sound pressure levels on velocity, with error bounds of two standard errors of estimate on either side of regression line for all downwind and near upwind results.

This velocity dependence function was applied to the original data and a graph of the equivalent peak level of a single four-axled vehicle train travelling at 120 km/h was plotted as a function of track to observer distance; this is shown in Fig. 6 together

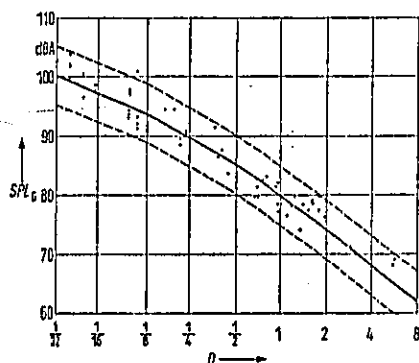


Fig. 6. Normalised peak A-weighted sound pressure level (SPL_G) as a function of distance from track in train lengths (D).

$$SPL_p = SPL_G + 10 \log \frac{A}{4N} - 20 \log \frac{l_v}{20} + 25 \log \frac{120}{Y} \pm 5 \text{ dBA.}$$

with the theoretical prediction and error bounds of two standard deviations.

The position of this curve with respect to the ordinate has been derived from the empirical data and Fig. 5 in particular. The predicted peak dBA noise level for any train at distance of up to eight train lengths and in the speed range 80 km/h to 160 km/h may be derived from this curve with the use of the following relationships:

Let SPL_p = be the predicted level
and SPL_G = be the level at the required distance given by Fig. 6,

then

$$SPL_p = SPL_G + 10 \log \frac{A}{4N} - 20 \log \frac{l_v}{20} + 25 \log \frac{Y}{120} \pm 5 \text{ dB.} \quad (6)$$

In practice this equation is satisfactory for trains in which the vehicles are not identical -- l_v and A are replaced by average values -- but the following expression may be used as an alternative

$$SPL_p = SPL_G + 10 \log \frac{AN}{4} - 20 \log \frac{l}{20} + 25 \log \frac{Y}{120} \pm 5 \text{ dB}$$

where l is the train length.

4. Discussion

In spite of the success of a line source model for the prediction of peak noise levels the noise profile measured when a train passes an observer is not predicted at all well. Qualitative improvement is achieved if convection effects are included in the line source model. Noise contours around moving trains were computed numerically and illustrate a characteristic closing up of the contours at the head of the train and a broadening of the contours at the rear. Inclusion of convection effects were not observed to alter the magnitude of the predicted peak sound pressure level over the whole speed range of interest although the peak level tended to be swept to the rear of the train. A further discrepancy may be due to the assumption that the rail-wheel radiators behave as simple monopole sources and there is now some evidence that this is unjustified. Finally the profiles are probably modified by wind effects.

Naturally this lack of correlation between predicted and observed profiles is a matter of some concern and until at least a statistical profile is generated we cannot predict the value of certain noise rating indices. Nevertheless the ability to predict peak noise levels has been of considerable benefit. Current work is concerned with improving the predicted noise profile and identifying noise indices which represent adequately the relatively mild impact of railway noise on the environment.

Acknowledgements

The author wishes to acknowledge the generous advice and encouragement that he received during the course of this work from Mr. R. BICKERSTAPPE, Dr. H. A. DELL and Mrs. B. WOODWARD. Mr. K. N. BUNTING and Mr. N. A. SHELLY are to be thanked for their technical assistance.

Thanks are due to the British Railways Board for permission to publish this paper.

(Received August 20th, 1972.)

References

- [1] BERANEK, L. L., Noise and Vibration Control. McGraw Hill, New York 1971.

12413

DEC 12 1973

ms: 2 AP

Journal of Sound and Vibration (1973) 28(2), 277-293

RECEIVED

NOV 29 1973

NOISE ABATEMENT PROGRAM
INFORMATICS INC.

CONTACT VIBRATIONS OF A WHEEL ON A RAIL

P. RANGANATH NAYAK†

*Bolt Beranek and Newman Inc.,
50 Moulton Street,
Cambridge, Massachusetts 02138, U.S.A.*

(Received 25 January 1973)

When a wheel rolls on a rail with a randomly wavy surface, the random waviness gives rise to a displacement input to the wheel and rail with a significant high-frequency ($f > 100$ Hz) spectral content. This displacement input excites the contact resonance of the system, wherein the mass of the wheel and an "equivalent mass" of the rail vibrate on the non-linear contact spring.

The purpose of this paper is to develop an analytical model for these high-frequency contact vibrations. The wheel is assumed to undergo only rigid-body motions, apart from the localized elastic deformation near the contact region. The rail is modeled as an infinite beam on a continuous, point-reacting foundation. With the rail roughness being assumed to be a locally stationary, Gaussian random process, a complete solution is presented to the linearized problem.

Three phenomena of interest are investigated in detail: plastic deformations, loss of contact, and the formation of corrugations on the rail. The effects of various wheel and rail parameters on these phenomena are explored.

1. INTRODUCTION

There has recently been an awakening of interest in the high-frequency vibrations of point contacting elastic bodies [1, 2, 3]. It is now established that the localized elastic deformations near the contact region play a central role in these vibrations, giving rise to a phenomenon known as contact resonance, wherein the masses of the contacting bodies vibrate on the non-linear contact spring. It is also established that in the case of rolling and/or sliding bodies, the roughness of the rolling bodies can excite this contact resonance to a sufficient degree so as to cause plastic indentations as well as loss of contact, which are of concern in studies of surface fatigue, friction, rolling noise, and the like.

Another phenomenon of interest in rolling contact is the formation of corrugations on the rolling surfaces, observed in such diverse situations as gear teeth [4], ball-bearing races [5] and railway track [6]. There has been much theorizing on what causes these corrugations, but there is now increasing experimental and analytical support [1, 2] for the belief that it is the surface roughness that is instrumental in causing corrugations, in conjunction with the contact resonance.

What little analytical work there has been to date on contact vibrations (vibrations involving contact deformations) has been concerned with two discs rolling against each other [2, 3]. This work has been motivated primarily by the need to explain phenomena observed in laboratory studies of rolling contact.

The aim of the present work is to investigate analytically the contact vibrations of a railway wheel on a rail. The problem is considerably more complex than that of the rolling discs, since one of the contacting bodies—the rail—is a continuous elastic system rather than a lumped one. Certain approximations make the problem tractable, however. The first of these is

† Now at Tata Engineering and Locomotive Company, Engineering Research Centre, Pimpri, P. F. Poona-18, India.

that the rigid-body motions of the wheel are negligible compared to the bending deflections of the rail. The second involves linearization of the problem, by means of a technique exploited by Gray and Johnson [3].

Three phenomena of considerable interest are analyzed in detail: plastic indentation of the rail, loss of contact, and the formation of corrugations on the rail. It is assumed that the rail roughness is a locally stationary, Gaussian random process with a known power spectral density. The effects on the phenomena mentioned of such parameters as the wheel load, rolling radius and rolling velocity, the rail linear density and bending rigidity, and the stiffness of the rail foundation are explored quantitatively.

The exact equations of motion for the wheel and rail are developed in section 2, and the approximations mentioned above are introduced. In section 3 the general solution of the linearized problem is presented. A quantitative investigation is made in section 4 for a particular roughness power spectral density frequently encountered in practice. In section 5, the analytical model and the results obtained from it are discussed, and recommendations are made for specific further analytical and experimental studies of the wheel-on-rail contact problem.

2. FORMULATION OF THE PROBLEM

Consider a wheel of mass M rolling on a rail with a rolling velocity V , as in Figure 1. The rolling surface (tread) of the wheel has a rolling radius R , and is conical. A steady load, P_0 , is applied to the axle of the wheel and is transmitted to the rail through the region of contact.

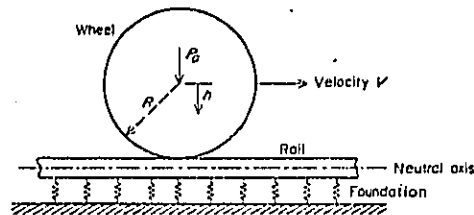


Figure 1. Wheel on a rail, with the rail modeled as a beam on a continuous, point-reacting elastic foundation. The displacement of the wheel center is h , and the bending deflection of the rail is y .

The rail may be modeled to a certain extent as an infinite beam (with bending rigidity EI) resting on a continuous, point-reacting foundation with a stiffness K_f . This model has its shortcomings, which will be discussed in section 5, but will suffice for a preliminary investigation of the problem.

When the surfaces of both the wheel and rail are smooth, the load transmitted to the rail is equal to P_0 . However, when the surface of the rail is rough, the roughness causes dynamic loads to be generated at the interface between the wheel and rail. These dynamic forces have been studied extensively in the low-frequency region ($f < 30$ Hz), where the wheel may be assumed to be rigid. However, when the rail roughness contains short-wavelength components, these give rise to high-frequency inputs to the contact. At sufficiently high frequencies, it is no longer permissible to assume the wheel to be rigid [2]. In fact, the local Hertzian deformation of both wheel and rail near the contact point becomes of the same order of magnitude as the input roughness, and plays a central part in the high-frequency dynamics of the system.

The problem of determining the dynamic contact loads can be formulated as follows. Let all displacements be measured from the configuration in which the wheel just touches the

rail, in the a
to the wheel
tion of the r
of the cont

where C is
on their el:
Figure 2 si
 R_2 , of the

Fig

N
the

an

st
ti

rail, in the absence of both roughness and a normal load. With an external load P_0 applied to the wheel, let the downward motion of the center of the wheel be h , and the bending deflection of the rail under the wheel be $y(0)$. The difference $z = h - y(0)$ is the Hertzian deflection of the contact if it is positive and is given by [7]

$$z = (P_0/C)^{2/3}, \quad P_0 > 0,$$

where C is a constant depending on the contact surface curvature of the wheel and rail, and on their elastic constants. When z is negative, it is the separation between the wheel and rail. Figure 2 shows C as a function of the wheel radius, R_1 , and the transverse radius of curvature, R_2 , of the rail head, for steel wheels on steel rails.

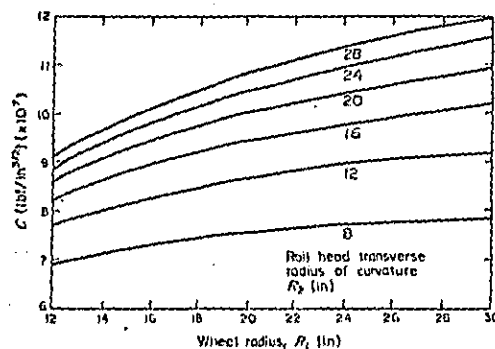


Figure 2. The Hertz constant C as a function of wheel radius and rail-head transverse radius of curvature.

Now if the rail surface has, in addition, a roughness w (measured upward from the rail), the Hertzian deflection is

$$z = w + h - y(0), \quad (1)$$

and the load between wheel and rail is given by

$$P = \begin{cases} Cz^{3/2} = C[w + h - y(0)]^{3/2}, & z > 0 \\ 0, & z < 0, \end{cases} \quad (2)$$

subject to a certain limitation on the frequency content of w as a function of time. This limitation is that no compressional resonances of the wheel or rail be excited.

Thus, the equation of motion for the wheel is

$$M\ddot{h} = P_0 - P = P_0 - C[w + h - y(0)]^{3/2}. \quad (3)$$

It will be implicitly assumed henceforth that $z^{3/2} \approx 0$ for $z < 0$.

The equation for the bending deflection, $y(x)$, is

$$EJ \frac{\partial^4 y}{\partial x^4} + m \frac{\partial^2 y}{\partial t^2} + K_r y = P\delta(x) = C[w + h - y(0)]^{3/2} \delta(x), \quad (4)$$

where m is the linear density (mass/unit length) of the rail and $\delta(x)$ is the Dirac delta function. The origin of the x -coordinate is centered in the contact region between the wheel and rail.

The general problem reduces to this: given the rail roughness w as a function of distance along the rail, s (measured from some fixed point), determine the contact load P as a function

tion.

EJ
as its
stigma-

the rail
dynamic
s have
may be
nents,
es, it is
forma-
nitude
of the

ss. Let
hes the

POOR
COPY

of time t , where $t = s/V$. As this problem appears to be highly intractable, it is necessary to fall back on the following limited problem, however: given that $w(s)$ is a stationary, Gaussian, random process with a known power spectral density (PSD), determine the PSD of the contact load P . It turns out, however, that even this limited problem is intractable because of the non-linear function appearing in equations (3) and (4). It is therefore necessary to further simplify the problem.

The first simplification ensues upon observing that if $w(s)$ is sinusoidal with wavelength λ , giving rise to a forcing frequency $f = V/\lambda$, then for reasonably large f , the linear impedance of the wheel is very large compared to the linear point impedance of the rail. Specifically, the impedance of the wheel is

$$Z_1 = i\omega M,$$

where $\omega = 2\pi f$, and that of the rail is

$$Z_2 = \frac{2K_{EQ}}{\omega} \left[\left(\frac{\omega}{\omega_{nr}} \right)^2 - 1 \right]^{3/4} (1 - i), \quad \omega > \omega_{nr},$$

where

$$K_{EQ} = (EI)^{1/4} (K_T)^{3/4}, \quad \omega_{nr} = (K_T/m)^{1/2}. \quad (5)$$

Typical values are $M = 3 \text{ lbf s}^2/\text{in}$, $EI = 1.73 \times 10^9 \text{ lbf/in}^2$, $m = 7.85 \times 10^{-3} \text{ lbf s}^2/\text{in}^2$ and $K_T = 3500 \text{ lbf/in}^2$, leading to $\omega_{nr} = 655 \text{ s}^{-1}$ and $K_{EQ} = 9 \times 10^4 \text{ lbf/in}$. Thus for $\omega > \omega_{nr}$ (i.e., $f \gtrsim 100 \text{ Hz}$), $|Z_1/Z_2| > 9$.

Despite the fact that the non-linearity generates harmonics of ω in the contact load, the preceding analysis suggests that, for reasonably high frequencies ($f > 100 \text{ Hz}$, say), the rigid-body motion of the wheel will be negligible compared to the bending deflections of the rail. It therefore appears heuristically justifiable to write the solution of equation (3) as

$$h = \bar{h} + \epsilon(t), \quad |\epsilon(t)| \ll \bar{h}, \quad (6)$$

where \bar{h} is the mean downward motion of the center of the wheel. Thus equations (1) and (4) become

$$z \approx w + \bar{h} - y(0) \quad (7)$$

and

$$EI \frac{\partial^4 y}{\partial x^4} + m \frac{\partial^2 y}{\partial t^2} + K_T y \approx C \delta(x) [w + \bar{h} - y(0)]^{3/2}. \quad (8)$$

The next step in the process of simplification is to linearize the non-linear forcing function in equation (8), in a manner identical to that used by Gray and Johnson [3] in a study of two discs rolling against each other. Specifically, $Cz^{3/2}$ is replaced by $P_0 + K_L(z - \bar{z})$, where K_L and \bar{z} are constants to be determined in such a way as to minimize the error in linearization. Note that \bar{z} is the mean value of z . Since z is given by equation (7), and since $\bar{w} = 0$ (by definition),

$$\bar{z} = \bar{h} - \bar{y}(0), \quad (9)$$

where $\bar{y}(0)$ is the mean value of the bending deflection of the rail under the wheel. Thus

$$z - \bar{z} = w - [y(0) - \bar{y}(0)]. \quad (10)$$

Thus the linearized form of equation (8) is

$$EI \frac{\partial^4 y}{\partial x^4} + m \frac{\partial^2 y}{\partial t^2} + K_T y = \delta(x) [P_0 + K_L \{w - [y(0) - \bar{y}(0)]\}]. \quad (11)$$

If one now writes

$$y(x, t) = y_1(x, t) + \bar{y}(x), \quad (12)$$

where $\bar{y}_1 = 0$, then \bar{y} and y_1 satisfy the following equations:

$$EI \frac{\partial^4 \bar{y}}{\partial x^4} + K_t \bar{y} = P_0 \delta(x), \quad (13)$$

and

$$EI \frac{\partial^4 y_1}{\partial x^4} + m \frac{\partial^2 y_1}{\partial t^2} + K_t y_1 = K_L (w - y_1) \delta(x), \quad (14)$$

which may be solved for $\bar{y}(0)$ and for the spectrum of $y_1(0)$. The spectrum of $(z - \bar{z})$ may then be obtained by combining equations (10) and (11) to obtain

$$z_1 \equiv z - \bar{z} = w - y_1(0, t). \quad (15)$$

3. THE LINEARIZED SOLUTION

Since the equations of motion have been linearized, y_1 and therefore $(z - \bar{z})$ will be Gaussian random processes when $w(t)$ is Gaussian, within the approximations involved. If σ_z^2 is the variance of $(z - \bar{z})$, the probability density of z is

$$p(z) = \frac{1}{\sigma_z \sqrt{2\pi}} \exp \left[-\frac{1}{2} \left(\frac{z - \bar{z}}{\sigma_z} \right)^2 \right]. \quad (16)$$

Now the contact load P is given by $P = Cz^{3/2}$ for $z \geq 0$ and $P = 0$ for $z < 0$. Thus the mean contact load is

$$P = C \int_0^{\infty} z^{3/2} p(z) dz = \frac{C\sigma_z^{3/2}}{\sqrt{2\pi}} \int_{-u_0}^{\infty} (u + u_0)^{3/2} \exp(-\frac{1}{2}u^2) du, \quad (17)$$

where

$$u_0 = \bar{z}/\sigma_z. \quad (18)$$

However, the mean contact load must equal the steady external wheel load, P_0 . Thus equation (17) yields one equation connecting \bar{z} and σ_z :

$$P_0 \sqrt{2\pi} / C\sigma_z^{3/2} = \int_{-u_0}^{\infty} (u + u_0)^{3/2} \exp(-\frac{1}{2}u^2) du. \quad (19)$$

A second equation is obtained by minimizing the error introduced in linearization. A measure of this error is

$$E = \int_{-\infty}^{\infty} [Cz^{3/2} - P_0 - K_L(z - \bar{z})]^2 p(z) dz.$$

When this error is minimized with respect to K_L , it is shown by Gray and Johnson [3] that the following constraint on \bar{z} , σ_z and K_L is obtained:

$$\frac{K_L \sqrt{2\pi}}{C\sigma_z^{3/2}} = \int_{-u_0}^{\infty} u(u + u_0)^{3/2} \exp(-\frac{1}{2}u^2) du. \quad (20)$$

The final constraint is obtained by solving equation (14), to obtain the PSD of first y_1 and then $(z - \bar{z})$, and then to obtain σ_z^2 . This can be accomplished as follows.

The mean bending deflection $\bar{y}(x)$ satisfies equation (13), which may be solved in a straightforward manner to yield

$$\bar{y}(0) = P_0/2\sqrt{2}K_{EQ},$$

which is the same as the bending deflection without roughness.

To obtain the PSD of y_1 , equation (14) is first solved when $w = w(\omega)\exp(-i\omega t)$, $\omega > \omega_{nr}$. The solution may be obtained in a straightforward fashion by Fourier transform techniques and is

$$y_1(0, t) = \frac{K_L w(\omega) i(1+i)}{(4K_{EQ}^* - K_L) + iK_L}, \quad \omega > \omega_{nr}, \quad (21)$$

where

$$K_{EQ}^* = K_{EQ}[(\omega/\omega_{nr})^2 - 1]^{3/4}. \quad (22)$$

From equation (15), $z_1 = (z - \bar{z})$ is found to be

$$z_1 = \frac{4K_{EQ}^* w(\omega)}{(4K_{EQ}^* - K_L) + iK_L}, \quad \omega > \omega_{nr}. \quad (23)$$

Thus the PSD of z_1 is given by

$$\phi_{z_1 z_1}(\omega) = \frac{16K_{EQ}^{*2}}{(4K_{EQ}^* - K_L)^2 + K_L^2} \phi_{ww}(\omega), \quad \omega > \omega_{nr}, \quad (24)$$

where ϕ_{ww} is the PSD of $w(t)$. The PSD of w in the frequency domain is related to its PSD in the wavenumber domain by

$$\phi_{ww}(\omega) = \phi_{ww}(k) \left| \frac{dk}{d\omega} \right| = \frac{1}{V} \phi_{ww}(k), \quad (25)$$

where $k = 2\pi/\lambda$ is the wavenumber (λ being the wavelength).

From equation (24), the variance σ_z^2 may be obtained:

$$\sigma_z^2 = \int_0^{\infty} \phi_{z_1 z_1}(\omega) d\omega, \quad (26)$$

where it has been assumed that the spectrum of w is one-sided.

This completes the analysis. For a given load, P_0 , and a given PSD, $\phi_{ww}(k)$, equations (19), (20) and (24)-(26) may be solved simultaneously to obtain K_L , \bar{z} and σ_z . Before proceeding to do this for a particular PSD, $\phi_{ww}(k)$, however, a restriction on equation (26) should be noted. The expression for $\phi_{z_1 z_1}(\omega)$ in equation (24) holds only for $\omega > \omega_{nr}$; for $\omega < \omega_{nr}$, the point impedance of the rail is that of a stiffness element rather than a mass. In these circumstances, it may be shown that the rigid-body motion of the wheel is no longer negligible; in fact it is the Hertzian compression that becomes negligible. Thus, even though $\phi_{ww}(k)$ may give rise to an input with a significant spectral content below ω_{nr} , thus causing significant dynamic contact loads, further discussion here will be concerned only with the region $\omega > \omega_{nr}$. Thus, equation (26) may be approximated by

$$\sigma_z^2 \approx \int_{\omega_{nr}}^{\infty} \phi_{z_1 z_1}(\omega) d\omega. \quad (27)$$

4. EXAMPLE OF A COMMON ROUGHNESS SPECTRUM

4.1. THE ROUGHNESS SPECTRUM

The frequency range of interest in the contact problem is approximately $f > 100$ Hz. For vehicle velocities under 300 ft/s, wavelengths giving rise to these frequencies are 3 ft and less. In this range of wavelengths, the PSD of the rail roughness is frequently found to be well approximated by [3]

$$\Phi_{ww}(k) = \frac{1}{Lk^4}, \quad (28)$$

where L is a constant. Small values of L indicate poor track quality; large values, good quality. With $k = \omega/V$, equations (25) and (28) may be combined to yield

$$\Phi_{ww}(\omega) = \frac{V^3}{L\omega^4}. \quad (29)$$

4.2. THE HERTZIAN DEFLECTION

Upon introducing equation (29) and equation (24) into equation (27), the following equation may be obtained:

$$\sigma_z^2 = \frac{1}{L} \left(\frac{V}{\omega_n} \right)^3 \int_0^{\infty} \frac{(\Omega^2 - 1)^{3/2} d\Omega}{\Omega^4 \{[(\Omega^2 - 1)^{3/4} - r_k]^2 + r_k^2\}}, \quad (30)$$

where

$$\Omega = \omega/\omega_n, \quad r_k = K_L/4K_{LQ}. \quad (31)$$

The integrals in equations (19) and (20) were evaluated numerically and are shown in Figure 3 as functions of $u_0 = \bar{z}/\sigma_z$. By combining these two curves, a relationship between $K_L/C\sigma_z^{1/2}$ and $P_0/C\sigma_z^{3/2}$ may be obtained, and is shown in Figure 4. Finally, the integral appearing in equation (30) is shown in Figure 5 as a function of r_k .

For purposes of numerical computation, the curves in Figures 4 and 5 and the curve for $K_L/C\sigma_z^{1/2}$ in Figure 3 may be approximated as follows:

$$K_L = 1.07(CP_0)^{1/2}/\sigma_z^{1/4}, \quad (32)$$

$$K_L = 3.1K_{LQ}(V/\omega_n)^{12/7}/L^{4/7}\sigma_z^{8/7}, \quad (33)$$

and

$$\bar{z} = -2.25\sigma_z + 2.35K_L\sigma_z^{1/2}/C. \quad (34)$$

These approximations are shown in the appropriate figures as dashed lines.

By using these approximate relations, a complete closed-form solution to the problem may be obtained. By combining equations (32) and (33), σ_z is found to be given by

$$\sigma_z = 3.3(K_{LQ})^{1.12}(V/\omega_n)^{1.92}/L^{0.64}(CP_0)^{0.56}, \quad (35)$$

Upon introducing this expression into equations (32) and (34), the following expressions are obtained for K_L and \bar{z} :

$$K_L = 0.79(CP_0)^{0.64}(\omega_n/V)^{0.48}L^{0.16}/K_{LQ}^{0.28}, \quad (36)$$

and

$$\bar{z} = (CP_0)^{0.92}(\omega_n/V)^{1.44}L^{0.48}/CK_{LQ}^{0.84} - 7.53K_{LQ}^{1.12}(V/\omega_n)^{1.92}/L^{0.64}(CP_0)^{0.56}, \quad (37)$$

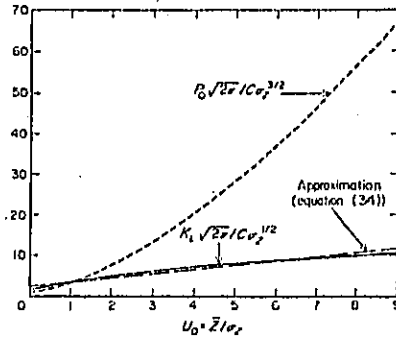


Figure 3. Integrals appearing in equations (19) and (20).

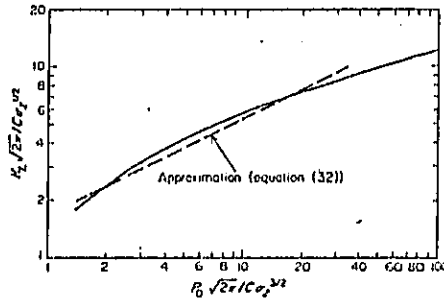


Figure 4. Relationship between $K_L / C \sigma_0^{3/2}$ and $P_0 / C \sigma_0^{3/2}$, obtained from Figure 3.

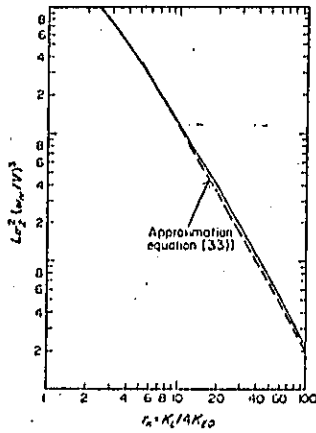


Figure 5. The variance σ_0^2 of the Hertzian compression as a function of the linearized contact stiffness K_L and the parameters ω_n , V and K_{20} .

4.3.

In
when
must

is gi
deri.

or, f

F

whic

T

Fig

C

in v

pro

val

S

var.

4.3. THE DYNAMIC CONTACT FORCE

In a non-linear analysis, the contact force would be obtained from equation (2). However, when the Hertzian deflection is obtained (as it is here) after linearization, the contact force must be obtained from $P = P_0 + K_L(z - \bar{z})$. Thus the dynamic contact force, defined by

$$P_d = P - P_0, \quad (38)$$

is given by $P_d = K_L(z - \bar{z}) \equiv K_L z_1$. Since z_1 is Gaussian with zero mean and has a standard deviation σ_{z_1} , P_d is also Gaussian with zero mean, and has a standard deviation

$$\sigma_{P_d} = K_L \sigma_{z_1}, \quad (39)$$

or, from equations (35) and (36),

$$\sigma_{P_d} = 2.61 (CP_0)^{0.08} (V/\omega_{hr})^{1.44} K_{LQ}^{0.84} / L^{0.48}. \quad (40)$$

Furthermore, the spectrum of P_d is clearly given by

$$\phi_{P_d P_d}(\omega) = K_L^2 \phi_{z_1 z_1}(\omega),$$

which, upon using equations (24), (28) and (31), reduces to

$$\psi_{P_d P_d}(\omega) = (K_L^2 / L) (V^2 / \omega_{hr}^2) \frac{(\Omega^2 - 1)^{3/2}}{\Omega^2 \{[(\Omega^2 - 1)^{3/4} - r_K]^2 + r_K^2\}}, \quad \Omega > 1, \quad (41)$$

This spectrum is shown in Figure 6 for a few values of r_K .

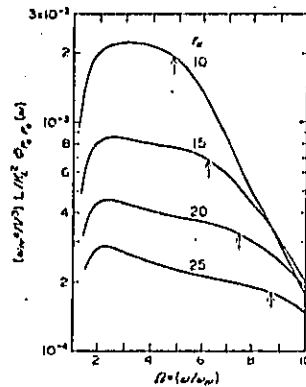


Figure 6. Dynamic contact load spectra. The arrows show the contact resonance frequency. $r_K \equiv K_L / AK_{LQ}$.

Certain statistics of the contact load are of interest in investigations of various phenomena in wheel-rail contact. These statistics are the probability of exceeding a specified value, the probability of being zero (indicating loss of contact), the frequency with which a specified value is exceeded, and the average size of "clumps" of such exceedances.

Since P_d is Gaussian with zero mean, the total contact load P is Gaussian with mean P_0 and variance $\sigma_{P_d}^2$. Thus the probability that P will exceed a specified value P_* is given by

$$\mathcal{P}_r(P > P_*) = \frac{1}{2} \operatorname{erfc} \left[\frac{(P_* - P_0) / \sigma_{P_d} \sqrt{2}}{1} \right]. \quad (42)$$

Similarly, the probability of loss of contact corresponds in the linearized problem to the probability that $P < 0$:

$$\mathcal{P}_{LC} = \mathcal{P}(P < 0) = \frac{1}{2} \operatorname{erfc}(P_0 / \sqrt{2} \sigma_{P_0}), \quad (43)$$

The quantity σ_{P_0} is given by equation (40).

The frequency with which P exceeds P_0 is given by [8]

$$v_{P_0} = \frac{1}{2\pi} \frac{\sigma_i}{\sigma_z} \exp \left[-\frac{1}{2} \left(\frac{P_0 - P_0}{\sigma_{P_0}} \right)^2 \right], \quad (44)$$

where σ_i is the standard deviation of the Hertzian compressional velocity; it is given by

$$\sigma_i^2 = \int_{\omega_{cr}}^{\infty} \omega^2 \phi_{12}(\omega) d\omega = \frac{V^3}{L\omega_{cr}^2} \int_1^{\infty} \frac{(\Omega^2 - 1)^{3/2} d\Omega}{\Omega^2 \{[(\Omega^2 - 1)^{3/4} - r_K]^2 + r_K^2\}}. \quad (45)$$

By combining equations (30) and (45), one may write

$$\frac{\sigma_i}{\sigma_z} = \omega_{cr} G(r_K), \quad (46)$$

where $G(r_K)$ is the function shown in Figure 7. The frequency of exceedances may now be obtained from equations (40), (44) and (46).

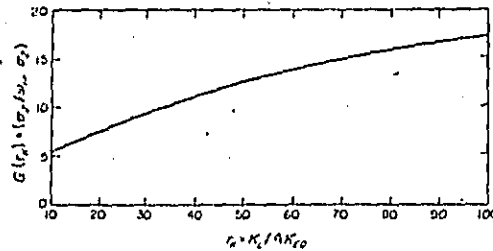


Figure 7. Quantity proportional to frequency of plastic indentations. See equation (46).

Estimates of the average number of exceedances (crossings of the level P_0) that occur in a clump can be obtained from the work of Lyon [9], discussed by Crandall [10]. The basic result is

$$n_{P_0} = \frac{1}{\sqrt{2\pi}} (1 - \lambda_1^2 / \lambda_0 \lambda_2)^{-1/2} \left(\frac{\sigma_{P_0}}{P_0 - P_0} \right), \quad (47)$$

where n_{P_0} is the average number of exceedances in a clump, and the parameters $\lambda_0, \lambda_1, \lambda_2$ are defined by

$$\lambda_n = \int_{\omega_{cr}}^{\infty} \omega^n \phi_{12}(\omega) d\omega. \quad (48)$$

Thus $\lambda_0 = \sigma_z^2$ and $\lambda_2 = \sigma_i^2$, the variance of the Hertzian compressional velocity.

By introducing equations (24) and (29) into equation (48), one obtains

$$\lambda_n = \frac{V^3}{L\omega_{cr}^{2+n}} \int_1^{\infty} \frac{(\Omega^2 - 1)^{3/2} d\Omega}{\Omega^{2+n} \{[(\Omega^2 - 1)^{3/4} - r_K]^2 + r_K^2\}}. \quad (49)$$

Fig range appro

In a of loss-

where C

4.4. six

Before sider a is perm equatio

yielding

which Equ

from w

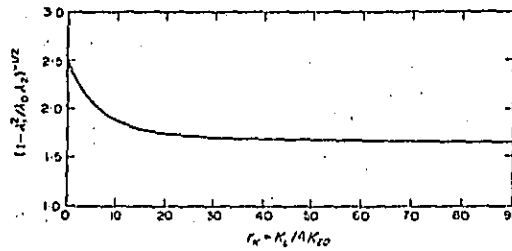


Figure 8. Quantity proportional to the mean clump size of plastic indentations. See equation (47).

Figure 8 shows the quantity $(1 - \lambda_1^2 / \lambda_0 \lambda_2)^{-1/2}$ as a function of r_K . It may be seen that in the range of r_K values of interest, the quantity does not vary much from a value of 2. Thus, approximately,

$$n_{P_0} \approx \sqrt{\frac{2}{\pi}} \sigma_{P_0} / (P_0 - P_0). \quad (50)$$

In an analogous fashion, it may be shown that within a linearized analysis, the frequency of loss-of-contact occurrences is

$$v_{L.C.} = \frac{\omega_{nr}}{2\pi} G(r_K) \exp[-\frac{1}{2}(P_0 / \sigma_{P_0})^2], \quad (51)$$

where $G(r_K)$ is given by Figure 7, and the average clump size of these occurrences is

$$n_{L.C.} \approx \sqrt{\frac{2}{\pi}} (\sigma_{P_0} / P_0). \quad (52)$$

4.4. SIMPLIFIED SOLUTION FOR $\bar{z} \gg \sigma_z$

Before proceeding to a discussion of the statistics of the contact load, it is helpful to consider a simplified analytical solution that yields useful insights. The simplification envisaged is permissible when $u_0 = \bar{z} / \sigma_z \gg 1$. This is precisely the region where the approximation of equation (32) is significantly in error. In this case, equation (19) may be approximated by

$$\frac{P_0 \sqrt{2\pi}}{C \sigma_z^{1/2}} \approx u_0^{3/2} \sqrt{2\pi}, \quad (47)$$

yielding

$$\bar{z} \approx (P_0 / C)^{2/3}, \quad (53)$$

which is the static Hertzian deflection.

Equation (20) may be approximated, after first integrating by parts, to obtain

$$\frac{K_L \sqrt{2\pi}}{C \sigma_z^{1/2}} = \frac{3}{2} \int_{-u_0}^{\infty} (u + u_0)^{1/2} \exp(-\frac{1}{2}u^2) du \approx \frac{3}{2} u_0^{1/2} \sqrt{2\pi}, \quad (48)$$

from which

$$K_L = \frac{3}{2} C \sqrt{\bar{z}} = \frac{3}{2} P_0^{1/3} C^{2/3}, \quad (49)$$

which is the stiffness of the Hertzian spring for small deflections. Typically, $K_L \approx K_{L0}$. It may thus be seen from equation (30) and Figure 5 that this solution is valid if $(V/\omega_n)^2/L$ is small enough so that $\sigma_z \ll \bar{\epsilon}$. In a given problem, the validity of this solution would be checked by calculating $\bar{\epsilon}$ from equation (53), r_K from equation (54), and then obtaining σ_z from Figure 5. If $\sigma_z \ll \bar{\epsilon}$ does not hold, the solution obtained in the preceding sections would be used.

5. DISCUSSION

The theoretical results of section 4 may be used to make a quantitative study of various phenomena of interest in wheel-rail interaction. Three specific phenomena discussed here are loss of contact, plastic indentations and the development of corrugations on the rail.

5.1. LOSS OF CONTACT

The probability of loss of contact is given by equation (43). It is clear that this probability is determined by the ratio of the static wheel load to the standard deviation of the dynamic contact force, P_0/σ_{r_d} , and that the probability decreases as the ratio increases. From equations (5) and (40), it may be seen that

$$P_0/\sigma_{r_d} \approx 0.38 P_0^{0.92} K_L^{0.09} L^{0.48} / V^{1.44} m^{0.72} (EJ)^{0.21}. \quad (55)$$

The effect of various parameters on the probability of loss of contact \mathcal{P}_{LC} is now clearly displayed. \mathcal{P}_{LC} increases as P_0 is decreased, L is decreased (track quality worsens), or as V , m or EJ are increased. The last two parameters are directly related to the cross-sectional area of standard track, and the conclusion is that as the track is made heavier, the probability of loss of contact increases. Of further interest is the extremely small influence of the foundation stiffness. The reason is clear: contact vibrations are generally of a high enough frequency that the rail mass-impedance is far greater than the foundation stiffness-impedance.

The frequency of loss of contact, ν_{LC} , is given by equation (51). From this equation and from Figure 7, it may be seen that ν_{LC} increases as ω_n or r_K increase, or as (P_0/σ_{r_d}) decreases. The quantity r_K may be determined from equations (31) and (36):

$$r_K \approx 0.2 (CP_0)^{0.64} (\omega_n/V)^{0.48} L^{0.16} / K_{L0}^{1.38}. \quad (56)$$

The variation of ν_{LC} with various parameters is complex and must be studied in each individual case. It is clear, however, that the product $\omega_n G(r_K)$ in equation (51) tends to counteract the exponential to a degree: an increase in P_0 or L , or a decrease in V , tends to increase the factor while decreasing the exponential.

The average clump size of loss-of-contact occurrences n_{LC} is found by combining equations (52) and (55). It is obvious that as the probability of loss of contact increases, so does the average clump size.

Example 1

Given $C = 8.9 \times 10^7$ lbf/in², $P_0 = 10^4$ lbf, $K_{L0} = 9 \times 10^4$ lbf/in, $\omega_n = 655$ s⁻¹, determine \mathcal{P}_{LC} , ν_{LC} and n_{LC} for average track, for $V = 3600$ in/s (300 ft/s).

L generally varies from $L \approx 5 \times 10^7$ in (good track) to $L \approx 5 \times 10^5$ in (poor track). With $L = 5 \times 10^6$, $\sigma_{r_d} = 4.7 \times 10^3$ lbf, from equation (40). Thus $P_0/\sigma_{r_d} = 2.12$, and, from equation (43), $\mathcal{P}_{LC} = 0.017$.

From equation (56), $r_K = 22.4$, and from Figure 7, $G(r_K) \approx 8.5$. Introducing these values into equation (51), one obtains $\nu_{LC} \approx 93$ s⁻¹; i.e., there are on the average 93 loss-of-contact occurrences per second. Finally, from equation (52), $n_{LC} \approx 0.38$. This last figure indicates that there is no tendency for the occurrences to be clustered together.

Example 2

Determine the effect of track quality on \mathcal{P}_{LC} , v_{LC} and n_{LC} for the case considered in example 1.

Variations in track quality are governed by variations in the parameter L . Using the results of example 1, one finds from equation (54) that

$$\frac{P_0}{\sigma_{P_s}} = 2.12 \left(\frac{L}{5 \times 10^6} \right)^{0.48}$$

As L varies from 5×10^5 (poor track) to 5×10^7 (good track), this ratio varies from 0.7 to 6.5, indicating the immense effect that track quality has on the dynamic contact load. From equation (43), \mathcal{P}_{LC} varies from 0.242 to practically zero. From equation (56), r_K varies from 15.5 to 32.5, and, from Figure 7, $G(r_K)$ varies from about 7 to about 10. Thus, from equation (51), v_{LC} varies from 570 s^{-1} to almost zero. From equation (52), n_{LC} varies from about 1.1 to about 0.12.

5.2. PLASTIC INDENTATIONS

Plastic indentation of the rail occurs when the contact load P exceeds a value P_p which depends mainly on the yield strength in shear of the rail material and on the contact surface curvature. Methods for determining P_p have been discussed elsewhere [11, 12]. For a 36-in wheel on an AREA 109 rail, P_p is in the neighborhood of 25 000 lbf.

The probability of plastic indentation is obtained from equation (42) upon setting $P_s = P_p$. For two given values of P_0 and P_p , this probability depends only on σ_{P_s} , which increases swiftly (see equation (40)) as V or m (rail linear density) are increased, or as L is decreased (track quality worsens).

Similarly, the frequency of indentations and their mean clump size may be obtained from equations (44) and (46), and (50), upon setting $P_s = P_p$.

Example 3

For $C = 8.9 \times 10^7 \text{ lbf/in}^{3/2}$, $K_{RQ} = 9 \times 10^4 \text{ lbf/in}$, $\omega_m = 655 \text{ s}^{-1}$, $P_0 = 2 \times 10^4 \text{ lbf}$, $P_p = 2.5 \times 10^4 \text{ lbf}$ and $V = 1200 \text{ in/s}$ (100 ft/s), determine \mathcal{P}_{P_s} (probability of plastic deformation), v_{P_s} and n_{P_s} for poor track.

For poor track, $L \approx 5 \times 10^5 \text{ in}$. From equation (55) (and from the results of example 2, section 5.1), $(P_0/\sigma_{P_s}) = 8.6$, or $\sigma_{P_s} = 2320 \text{ lbf}$. From equation (42), $\mathcal{P}_{P_s} = 0.015$. From equation (55), $r_K = 41$, and from Figure 7, $G(r_K) \approx 12.5$. Then from equations (44) and (46), the frequency of plastic indentations is $v_{P_s} = 130 \text{ s}^{-1}$. From equation (50), the average clump size of indentations is found to be small, indicating a random distribution of indentations along the track.

5.3. RAIL CORRUGATIONS

The formation of corrugations on the rail is closely tied to the occurrence of plastic indentations. In a general way, it is clear that when indentations occur, they change the spectrum of the rail roughness. A subsequent wheel rolling on the track may respond to a higher level than the first one, causing the indentations to both deepen as well as propagate along the track. Thus corrugations may be considered to arise from an instability in the wheel-rail system.

The question of major interest is what differentiates rails on which corrugations occur from those which suffer stable, non-propagating plastic indentations.

Several hypotheses are available, none well-established. In the case of rolling discs that develop corrugations, the spectrum of the dynamic contact force is narrow-band, implying

that the contact force is almost sinusoidal with a slowly varying amplitude. In this case, plastic indentations will tend to cluster around locations where the force envelope crosses the critical load P_p . These clusters cause a large local change in the disc roughness PSD at precisely the frequency at which the disc dynamic response is high, so that subsequent rolling will tend to corrugate the discs locally. In this case, the probability of corrugation is closely related to the average clump size of plastic indentations, n_p . When the clump size is large, the discs have a greater opportunity to build up an almost steady-state response during subsequent rolling. When n_p is small, the discs suffer only a transient response, and the clumps tend not to propagate. What clump size is critical must depend on the rise time of the transient response of the system, which remains to be investigated.

In the case of wheels on rails, the numerical examples given above indicate that n_p is small; i.e., that plastic indentations do not tend to cluster together. The reason for this is apparent from an examination of the dynamic force spectra in Figure 6: they are not narrow-band. Bending waves in the rail propagate energy away from the contact and heavily damp the system response.

The fact that the system response spectrum is broad does not necessarily signal the demise of the mean clump size hypothesis for the formation of corrugations. The factor $\sigma_{P_p}/(P_p - P_0)$ appearing in the expression for n_p may be considerably larger than the values obtained here for at least two reasons.

First, the range of values assumed here for the track quality parameter L is based on measurements averaged over fairly long sections of track. This may tend to smooth out rough sections of track which are short by conventional standards but nevertheless long enough to cause the wheel/rail system to build up a high response. It seems intuitively obvious that, given a long section of track, the probability of corrugation is not uniform along it—over a long period of time, the entire track does not corrugate if part of it does. This suggests that local variations in roughness spectra are of importance; these have not as yet been measured.

Second, although the mean contact load is, indeed, P_0 , there are superposed on this low-frequency dynamic loads due to suspension resonances. The frequency of these resonances is low enough compared to contact vibration frequencies that one may consider the mean contact load (averaged over many contact vibration cycles) to be slowly varying in time. There will thus be periods of time when the quasi-static (static + low-frequency dynamic) load will be close to the critical plastic load, P_p . The number of exceedances of the total contact load (including high-frequency variations) above P_p , as well as their average clump size n_p , will then dramatically increase, perhaps sufficiently to allow corrugations to start.

An alternative hypothesis is that even when the mean clump size of exceedances is small, corrugations may occur if the frequency of these exceedances is comparable to the frequency at which the response spectra of Figure 6 have their maxima. The reasoning here is that whether or not the plastic indentations tend to cluster together, they change the rail roughness spectrum, the largest change being at the mean indentation frequency. If this frequency lies in the range between, say, $2\omega_{cr}$ and $4\omega_{cr}$, the response of subsequent wheels will tend to increase substantially at this frequency.

It hardly needs stating that the preceding discussion is at present entirely hypothetical. No data are as yet available which may be used to test these theories, and much experimental work needs to be done. It is worth remarking however, that the basic mechanism of corrugation appears to lie in the excitation of contact vibrations by the roughness of the rolling bodies, regardless of the specific mechanical system one has in mind. What is learned from any one system is likely to be universally applicable in its essentials.

5.4. THE

A que
phenom
contact
which, fi

A clo
to the co
No peak
in the ra

It is in
a wavele
corrugat

Some
the appi
corresp
the spec
say by h

Furth
spectru
become
are, ind
of linea

5.5. sru

Befo
in the a
far sup

One
known
the rail

where
arising
groun

Thei
any qu
the rail
more c
deflect
will be
indent

And
the co
occur,
force
of dif
sectio

5.4. THE DYNAMIC CONTACT FORCE SPECTRA

A question of interest regarding the spectra shown in Figure 6 is how well they display the phenomenon of contact resonance mentioned in the introduction and observed in the rolling contact of two discs [3]. It may be seen that the spectra peak between $\Omega = 2$ and $\Omega = 4$, which, for typical values of ω_{nr} , corresponds to a frequency between $f \approx 200$ Hz and $f \approx 400$ Hz.

A closer examination of the spectra, however, indicates that the peak does not correspond to the contact resonance, the frequency of the latter being given approximately by $\Omega = r_k^{2/3}$. No peak appears in the spectrum at this value of Ω because of the large amount of damping in the rail.

It is interesting to observe that at a speed of $V = 50$ ft/s, the peak frequency corresponds to a wavelength between 1.5 in and 3 in, which compares well with the wavelength of observed corrugations on rails [6].

Some reservations need to be expressed regarding the spectra shown in Figure 6. First, the approximation of a rigid wheel (in comparison with the rail) is invalid at values of Ω corresponding to wheel rim resonances, likely to be $\Omega > 3$. Near these resonant frequencies, the spectra shown will overestimate the true spectra, although it is not at present possible to say by how much.

Furthermore, it is not intended that Figure 6 should convey the impression that the load spectrum is small for $\Omega < 1$. This is the region in which the rigid-body modes of the vehicle become important, and in which the present analysis is inappropriate. Large spectral levels are, indeed, to be expected for $\Omega < 1$, but these must be studied by the well-known techniques of linear lumped-system analysis.

5.5. SHORTCOMINGS OF THE ANALYTICAL MODEL USED

Before concluding, it is appropriate to offer some brief comments on various shortcomings in the analytical model developed in section 2, the elimination of which is likely to lead to a far superior predictive analysis.

One shortcoming lies in modeling the rail as a beam on an elastic foundation. It is, in fact, known [13] that a better (but not quite complete) formulation of the equation of motion of the rail than that given in equation (4) is

$$EI \frac{\partial^4 y}{\partial x^4} + (m + m_a) \frac{\partial^2 y}{\partial t^2} + g \frac{\partial y}{\partial t} + K_t y = P\delta(x),$$

where m_a is an "added mass" arising from the ties, ballast, etc., and g is a damping coefficient arising from energy losses in the track structure due to both friction and radiation into the ground.

There is not enough information available at present on the parameters m_a and g to support any quantitative statements. Qualitatively, however, it appears that the point impedance of the rail will be higher than for the beam-on-elastic-foundation model. As a consequence, more of the roughness will be taken up by Hertzian compression rather than by rail bending deflection. Furthermore, because of the increased mass, the rail resonance frequency ω_{nr} will be decreased, thereby causing increases in the probabilities of loss of contact and plastic indentation, as well as in the mean frequency and clump size of indentations.

Another parameter neglected in the analysis is the tractive force being transmitted through the contact. This force significantly decreases the normal load at which plastic indentations occur, for values of the coefficient of friction normally encountered. In addition, the tractive force is not symmetric with respect to the direction of rolling, thus leading to the possibility of differences in the likelihood of corrugations, depending on whether vehicles on a given section of track are accelerating, cruising at a steady speed, or being braked. Such differences

have been observed by Carson and Johnson [1] in their study of the formation of corrugations on rolling discs.

A further assumption in the formulation of the problem is that the entire contact region sees the same rail roughness. This assumption has been shown by Gray and Johnson [3] to be untenable. They show that parallel profiles along the rolling surfaces may be uncorrelated to a remarkable extent, even at very small separations of the profiles. This lack of correlation leads to a reduction in the mean input seen by the contact region, the amount of attenuation depending on the cross-correlation of parallel profiles. For the wheel-on-rail problem, no data on cross-correlation are available, but it may be noted that the assumption of perfect correlation between parallel profiles used here is a conservative one, leading to overestimates of P_p , \mathcal{P}_{LC} and n_p .

Finally, the assumption that the wheel is rigid except for the Hertzian deflections also becomes untenable at higher frequencies. At some frequency, the rim of the wheel has its first inplane ring bending resonance. The plate of the wheel constrains the rim to a certain extent, but a lower bound on the first resonance may be obtained from [14]

$$f > \frac{C_1 h}{2\pi r^2},$$

where C_1 is the speed of longitudinal waves in the wheel material, h is the radial thickness of the rim (approximated as a ring with a rectangular cross-section), and r is the radius of the rim. Typically, this frequency ranges from 300 Hz up. Near this resonant frequency (and near higher resonant frequencies), the impedance of the wheel may no longer be assumed to be large compared to that of the rail; in fact, the impedance becomes quite small, and as a consequence, much of the roughness is taken up in bending of the rim rather than in Hertzian compression. Near wheel resonances, therefore, the spectrum of the dynamic contact force given by equation (41) is incorrect, the values being too high.

Even in the presence of a wheel resonance, the problem may be solved by replacing the wheel by a linear second-order system representing the mode. Such an analysis has not yet been made.

5.6. CONCLUDING COMMENTS

In order to extend the analysis presented here so that it yields a reasonably accurate predictive scheme, much work will have to be done:

- (a) a study of the PSD of rail roughness at short wavelengths, and of the variation of this PSD along the rail,
- (b) a study of the cross-correlation of parallel profiles,
- (c) a study of the high-frequency dynamic model of a rail on its foundation,
- (d) a study of the transient response of the wheel-on-rail system to non-stationary inputs,
- (e) a study of the effect of tractive forces in the contact region on the speed of development of corrugations,
- (f) a study of the effect of contaminants such as water and oil on the dynamic response of wheels on rails.

A further question worth pursuing is the effect of the low-frequency dynamic load spectrum on such phenomena as plastic indentations, corrugations and loss of contact, briefly discussed in section 5.3. This low-frequency spectrum contains large peaks at certain resonant frequencies, so that the actual wheel load fluctuates slowly (compared to contact vibration frequencies) in an almost periodic fashion. These fluctuations may amount to a significant fraction of the mean wheel load. As far as the contact vibrations are concerned, the low-

fre
high
wh
is s
l
the
of i

un

1.

2.

3.

4.

5.

6.

7.

8.

9.

10.

11.

12.

13.

14.

frequency load variations are almost quasi-static, the wheel load being alternately low and high. When this quasi-static load is low, the probability of loss of contact is further increased; when it is high, the probability of plastic deformations and of the formation of corrugations is similarly increased.

It is hoped that the preliminary results obtained here will spur a vigorous investigation of these and other high-frequency wheel/rail contact phenomena, since they appear likely to be of importance in the development of future high-speed wheeled transportation.

ACKNOWLEDGMENT

This work was supported in its entirety by the United States Department of Transportation, under Contract No. DOT-FR-10031; this support is gratefully acknowledged.

REFERENCES

1. R. M. CARSON and K. L. JOHNSON 1971 *Wear* 17, 59-72. Surface corrugations spontaneously generated in a rolling contact disc machine.
2. P. R. NAYAK 1972 *Journal of Sound and Vibration* 22, 297-322. Contact vibrations.
3. G. G. GRAY and K. L. JOHNSON 1972 *Journal of Sound and Vibration* 22, 323-342. The dynamic response of elastic bodies in rolling contact to random roughness of their surfaces.
4. E. W. LANDEN 1968 *Transactions of the American Society of Lubrication Engineers* 11, 6-11. Slow speed wear of steel surfaces by thin oil films.
5. A. PALMGREN 1945 *Ball and Roller Bearing Engineering*. Philadelphia: SKF Industries.
6. BRITISH RAILWAYS 1954 *Bibliography on Corrugations of Rails*. Derby: British Railways Research Department.
7. S. TIMOSHENKO 1951 *Theory of Elasticity* (second edition). New York: McGraw-Hill Book Company, Inc.
8. S. O. RICE 1945 *Bell System Technical Journal* 23, 282-332; 24, 46-156. Mathematical analysis of random noise.
9. R. H. LYON 1961 *Journal of Acoustical Society of America* 33, 1395-1400. On the vibration statistics of a randomly excited hard-spring oscillator II.
10. S. H. CRANDALL 1970 *Journal of Sound and Vibration* 12, 285-299. First crossing probabilities of the linear oscillator.
11. K. L. JOHNSON and J. A. JEFFERIS 1963 *Proceedings of the Institution of Mechanical Engineers Symposium on Fatigue in Rolling Contact*. Plastic flow and residual stress in rolling and sliding contact.
12. K. L. JOHNSON 1963 *Proceedings of the Institution of Mechanical Engineers Symposium on Fatigue in Rolling Contact*. Correlation of theory and experiment in research on fatigue in rolling contact.
13. W. E. GELSON and E. A. BLACKWOOD 1965-1966 *Proceedings of the Institution of Mechanical Engineers Symposium on Interaction of Vehicle and Track*. Contributed discussion.
14. J. P. DENHARTOG 1956 *Mechanical Vibrations* (fourth edition). New York: McGraw-Hill Book Company, Inc.

E22Y19

INTER-NOISE 73
 TECHNICAL UNIVERSITY OF DENMARK
 COPENHAGEN, 22-24, AUGUST 1973

NOISE INSIDE AND OUTSIDE VEHICLES AND FROM RAILWAY LINES

L. Willenbrink

Munich Research Center of German Federal Railways (DB)

1. Preface

Traffic produces noise. As one of the producers of transportation the German Federal Railways are engaged to control the sound radiation of their rolling stock /1/. The results of manifold tests in this matter are concisely reported in the following.

2. Noise inside vehicles

2.1. Locomotives: High sound levels in driver's cabins affect concentration and hearing. In steam locos and some older electric or diesel engines there were sound levels of about 100 dB(A) at full power, in modern locos only 72 up to 82 dB(A). After having 100 dB(A) in the motor cells those low sound levels were attained by special sound and vibration reducing double panelled side walls and floors or even a completely floating cabin for shunting locos.

2.2. Passenger coaches: For good driving comfort in passenger coaches should be kept an upper limit of max. 80 dB(A), but there is a lower limit, too: down 60 dB(A) there will be disturbances of the homyness by then audible talks between other passengers. Fig.1 shows typical third-octave spectra in the compartments for three speeds. Weighting them with curve A it follows, that further noise controlling steps were to have effects in the range between 250 Hz and 2 kHz. The following sound levels at 120 km/h inside coaches are standard: sleeping cars 60 dB(A), high comfort coaches 65 dB(A), normal express coaches 70 dB(A), suburban traffic cars 75 dB(A). In the compartments near the bogies there are 5 dB(A) more than in those in the middle of a car when running with 160 km/h. In tunnels

INTERNAL NOISE

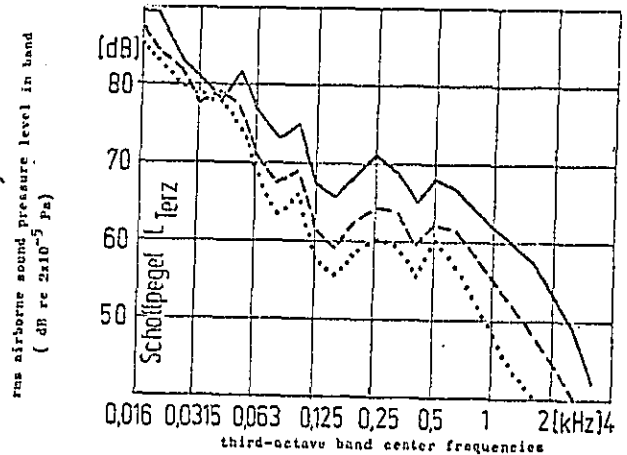


Fig. 1: Noise in a 2-cl.-coach riding on ballast-bed track
 — 160 km/h, 72 dB(A), - - - 120 km/h, 66 dB(A), 80 km/h, 62 dB(A)

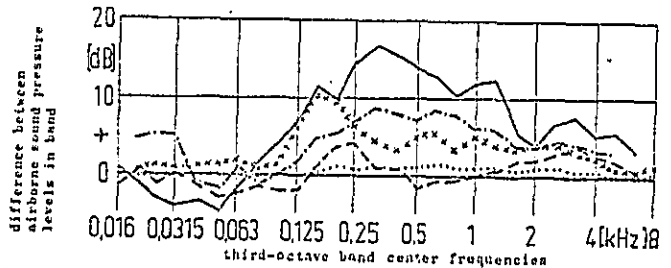


Fig. 2: Noise differences ΔL in some cars at different conditions
 — ΔL (block braked/unbraked), 120 km/h, sleeping car
 - - - ΔL (disc braked/unbraked), dito, same type of car construction
 - · - ΔL (run in tunnel/run on surface), different cars and speeds averaged
 · · · · ΔL (new/ground and polished rails), run in tunnel, different speeds averaged

the sound level increases for 6 dB(A) (s. Fig. 2). Especially for sleeping cars the disc brakes meant big progress, since there is asymptotic braking noise no more, whereas the block brakes let grow sound levels for about 13 dB(A) (s. Fig. 2).

No significant differences were measured between run on wooden and run on concrete sleepers in ballast-bed track. But the ballastless tracks in some underground systems may cause increasing sound levels in the cars due to the missing sound absorbing effect of the ballast bed or especially if natural frequencies of the concrete parts are not damped after excitation by the running train (s.3.2.3). Corrugated rails and wheel-flats cause considerably raisings of the sound levels in the cars (more than 10 dB(A)), but also do only rugged rail surfaces as on new rails. Fig.2 shows the effect of just ground rails and of ground and by use polished rails.

3. Noise outside vehicles and from railway lines

3.1. Airborne sound

3.1.1. Normal surface lines

3.1.1.1. Noise event sound levels: Fig.3 shows third-octave spectra of the noise of passing trains (no railcars) at different distances. The diminution of the wayside noise in accordance with distance is higher than expected by theory. By doubling distance from a line sound source - as a train is representing - one is expecting a decrease of 3 dB; but there were measured 5 dB(A) at a height of 1,2 m above ground level equal to rail level, for distances between 15 m and 100 m, and even more decrease for longer distances. At higher points above ground there are some higher levels due to the lower influence of ground absorption: in a height of 3,5 m instead of 1,2 m there were +1 to +3 dB(A) at 25 m distance. Doubling speed between 60 km/h and 200 km/h causes 10 dB(A) higher sound levels; changed are mainly the band levels in the kHz-range. If there are corrugations on the rails or wheel-flats, the wayside noise increases considerably up to 15 dB(A). At the faster trains over 80 km/h the main sources are both wheels with bogies and rails, so that the locomotives noise does not exceed the noise of the cars; but at slower trains there are in addition to that the exhausts and cooling vents. Cars of the same type may have a variation of ± 3 dB(A) due to differential repair. 90% of the measured trains had generated sound levels within ± 2 dB(A) around the

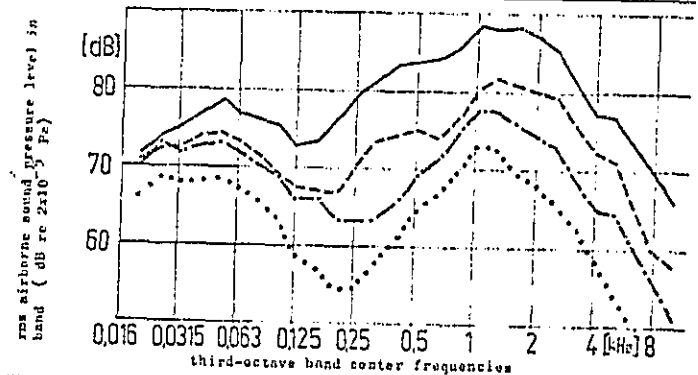


Fig. 3: Noise of passing trains (no railcars), 120 km/h

distance	height	Sound Level (dB(A))
10 m	2 m above rail level	96 dB(A)
25 m	1,2 m	89 dB(A)
50 m	1,2 m	84 dB(A)
100 m	1,2 m	79 dB(A)

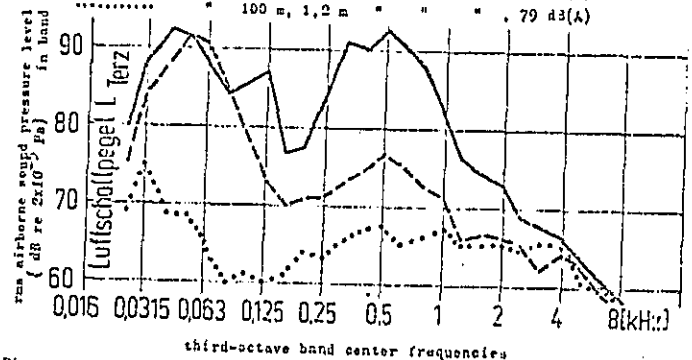


Fig. 4: Bridge noise, electric test loco, 80 km/h, distance 25 m, height 1,6 m above ground level

Track Type	Sound Level (dB(A))
steel-made sheet-girder bridge, direct rail fastening	95 dB(A)
same bridge, but with ballast-bed track	82 dB(A)
normal surface track with ballast-bed	76 dB(A)

values given in Fig. 3, but new electric multiple-unit rapid transit stock with an axle load of 12 t showed levels up to 10 dB(A) lower; the typical hump in the kHz-range of the spectra of normal trains was missing.

3.1.1.2. Equivalent continuous sound levels. The reported noise event levels cause the following equivalent continuous sound levels valid for a distance of 25 m and a cycle of 10 trains per hour:

long-line traffic (high speed and/or long trains)	75 dB(A)
regional traffic (middle speed, short and long trains)	70 dB(A)
suburban traffic (middle speed, short and few goods trains)	65 dB(A)

subway and streetcar 60 dB(A).

Doubling the cycle causes 3 dB(A) more, doubling the speed 3 dB(A) for the mentioned new multiple-unit stock to 7 dB(A) for normal trains and doubling the length of each train somewhat less than 3 dB(A); the contribution of the level rise and slope when the train is coming and going is to be regarded.

3.1.2. Screens: Since wheels with bogies and rails are the main noise sources, the direct sight on them from the immission point has to be interrupted. So the sound absorbing effect of a screen in a distance of 2,5 m from the middle of the track and with a height of 1,5 m above rail level is calculated to be about 15 dB(A) for train noise spectra and distances up to 100 m in a plain. But those calculated effects of screens are very unsafe /2/ because of the influence of some parameters hardly to be caught, as wind or temperature gradients, although some of those calculating methods are developed after field trials /3/. If the screens are radiating secondary airborne noise, because they are mounted on vibrating structures, their effect will be reduced.

3.1.3. Bridges: It is desired, that bridges do not radiate more noise when overrun as the normal track does. Fig. 4 shows, how far away from that desire an older steel-built bridge was been with its direct rail fastening; it also shows the big progress after laying on that bridge a ballast-bed track. A modern steel-made hollow-box-type bridge with ballast-bed track attained in fact the just reported desire and so do some concrete-made bridges when fitted with ballast-bed track. The sound emission of large bridge parts can be reduced by sandwich construction, by stiffeners and by big masses as for instance ballast-bed. The rubber-layers between concrete-

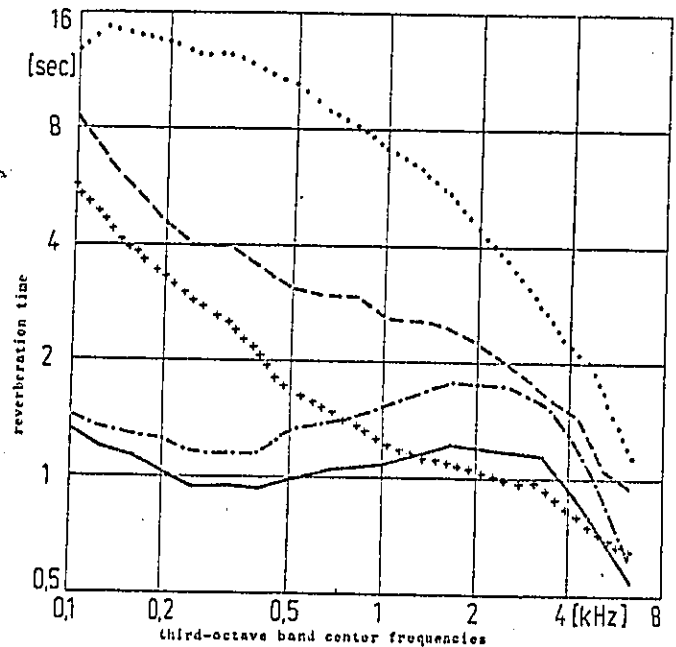


Fig. 5: Reverberation time in an underground station of around 200m x 22m x 5m

- in bare concretework situation
 - dito, but with two ballast-bed tracks
 - in completed situation with damping panels and ceiling
 - dito, but instead of the ballast-bed tracks ballastless ones (scale)
 - +++++ in bare concretework situation with two ballast-bed tracks and 0,15 persons/m² on the 7 m broad middle platform (calculated).
- } (measured)

made track plates and a steel-made bridge construction reduced certainly the vibration propagation into the steel construction, but the plates themselves now vibrated and radiated noise.

3.1.4. Underground railways. It is possible, to hold the sound level in modern subway cars under 75 dB(A), when riding with 60 km/h in the tunnel on ballast-bed track (but s. 2.2.).

A reverberation time of 2 sec in underground stations seems to be sufficient for tolerable sound levels (ca. 80 dB(A)) affecting on waiting people, when trains are arriving or starting. Fig. 5 shows the change of the reverberation time after inserting some different sound absorbing surfaces in a large tunnel station as ballast-bed tracks, special panels and hanging ceilings. Waiting people have a sound absorbing effect, too.

3.2. Structureborne sound (vibration in the audible range) /4/. Railway lines are producing not only airborne, but also structureborne sound, which may become a problem, especially for underground railways in housing areas. No troublesome noise should be radiated by vibrating walls into the rooms of neighbored or underrun buildings. Since the higher frequencies mostly are sufficiently damped by the soil, special structureborne sound insulating track constructions must have their effect mainly in the range between about 25 Hz to about 160 Hz. The structureborne sound propagation in the soil varies very much and is difficult to determine; so it seems to be better to see for the effects of special track constructions at test points on the side wall of the tunnels, with horizontal vibration direction. To do that at only one point for every construction is completely insufficient and let come up errors; simultaneous tests at six similar, max. 5 m between each other distanced points on the side wall of a ballast-bed track tunnel showed a variation in band levels of the same quantity as was the - only at one point measured - effect of some special ballastless track constructions. Fig. 5 shows the variation between five of those six points; the sixth has had unexplicably far away levels. Searching for track constructions, which are better insulating structureborne sound than the conventional ballast-bed, the following results are secured:

3.2.1. Different heights of ballast-bed: Increasing the ballast-height under sleepers from 30 cm up to 50 cm or 70 cm or 45 cm

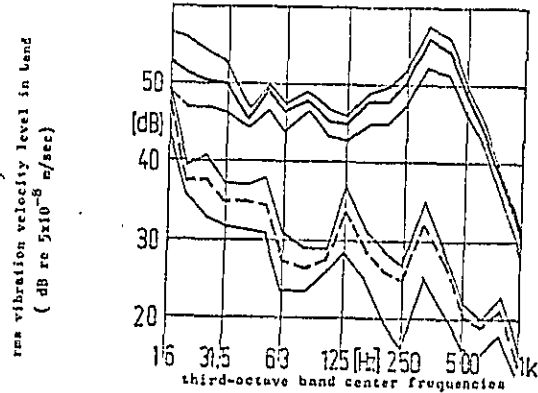


Fig. 6: Variation and energy middle of the structureborne sound velocity levels of five similar and simultaneous measured test points at the side wall of the same tunnel; vibration direction horizontal; electric multiple-unit stock, 60 km/h.

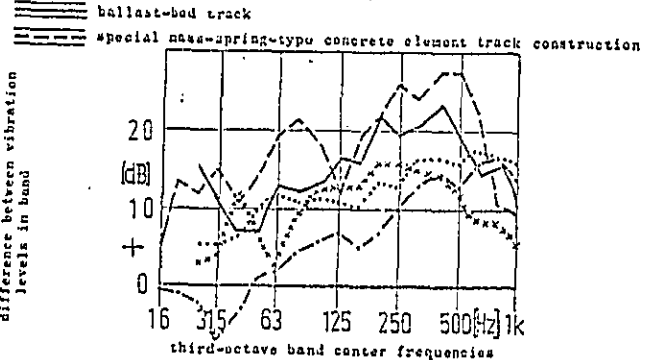


Fig. 7: Effects ΔL at the tunnel side wall test points of several enactments:
 — ΔL (ballast-bed track/mass-spring-type concrete tub track)
 - - ΔL (" " " / " " " elements " (s.Fig.6))
 - · - ΔL (" " " / ballast-bed track over threefold rubber mats)
 ····· ΔL (unground/ground rails), ballast-bed track
 ······ ΔL (poor/good wheel surface), " " "

with 25 cm sand did not show any effect using unground rails. It must not be concluded that the height is allowed to be less than 30 cm under sleepers.

3.2.2. Rubber layer under ballast-bed: A 3 cm thick composition of three profiled, by fulling work energy consuming rubber mats, which were placed under the ballast-bed, showed an improvement which was slightly increasing from 50 Hz up to higher frequencies (10 dB at 250 Hz) (s. Fig.7).

3.2.3. Track constructions of mass-spring-system type: The vibrations excited in the rails by running trains are considerably insulated, if they have to pass on their way into the tunnel construction a mass-spring-system, whose natural frequency is below the audible range as well as sufficiently far away from the wheel rotation frequency, say about 10 Hz. That requires high masses, since the spring depression is limited by the permissible vertical motion of the rails. Fig.7 shows the effects of two types of such systems, one of them having a recess at third-octave band 125 Hz. Here the natural frequency of the concrete-made, exchangeable elements was excited; since it was only slightly damped, it produced a considerable increase of airborne sound level in the cars.

3.2.4. Corrugated or rough new rails and wheel-flats are able to let grow the structureborne sound levels so, that the effects of expensive special track constructions are nullified (s.Fig.7).

3.2.5. Thickness of the tunnel walls: Comparing the measured vibration velocity levels on the tunnel side walls with the thicknesses shows a reduction of about 10 dB for a thickness growth of 50 %.

3.2.6. Propagation of structureborne sound.

3.2.6.1. In tunnel walls: The temporal run of the structureborne sound level at a test point on the tunnel wall when a train is passing shows two different zones of the absorption rate: from the exciting axle to a distance of 10 m the octave band levels in the range between 63 Hz and 1 kHz decrease with a rate of about 2 dB/m, farer away with 0,5 dB/m. Hence it follows, that it will be sufficient to extend the at this time known special track constructions with their effect of around 10 dB for only 10 m beyond the projection of the buildings to protect on the tunnel

axis.

3.2.6.2. At the surface: The propagation of the structureborne sound through the soil depends on too much parameters difficult to determine, such as wetness, type and percentage of rock, elasticity. Today we are not able to give secured values in face of such outcomes as for instance, that the third-octave band levels of eight quite similar and simultaneous test points in the undisturbed soil of a meadow varied up to 15 dB.

4. Literature

- /1/ C. Stüber, Schienenverkehrslärm und Lärm gewerblicher DB-Anlagen. Die Bundesbahn, Heft 13/14/1972 S. 821 ff.. (Dort viele weitere Literaturangaben).
- /2/ Fleischer und Schorr, Lärmbekämpfung mit Schallschirmen. Wärme, Kälte, Schall Nr. 2/August 1971 S. 3 ff.
- /3/ Rathe, ORE-Bericht E 82 Nr. 3 "Ausbreitung von Eisenbahnlärm", ORE, Utrecht.
- /4/ Hauck, Willenbrink und C. Stüber, Körperschall- und Luftschallmessungen an unterirdischen Schienenbahnen. ETR Heft 7/8 1972, S. 289 and continuation in a new issue of summer or autumn 1973.

NOISE-CON 73
Bender and Remington, 1

THE INFLUENCE OF RAILS ON TRAIN NOISE

by

Erich K. Bender and Paul J. Remington
Bolt Beranek and Newman Inc., Cambridge, Mass. 02138

Presented at

NOISE-CON 73
Washington, D.C.

October 15 - 17, 1973

12199

732173

1. INTRODUCTION

The resurgence of rail rapid transit in the U.S. and abroad, the innovation of high-speed long distance rail transit in Europe, Japan, and the U.S.; and a recently developed concern for the environment have resulted in renewed emphasis on the interaction of steel wheels with steel rails and the noise and vibration that it causes. Even though the "clickety-clack" noise can be largely eliminated through the use of continuously-welded rail, significant levels of noise and vibration are still generated by the microroughness on wheels and rails, the sideways impact of wheel flanges against rail heads, and the intense squealing or screech encountered in small radius turns.

The purpose of this paper is to analyze one form of the wheel-rail interaction, attributable to wheel and rail roughness, and to estimate the rail response and sound radiation. This is, of course, but one part of the problem, others being concerned with different excitation mechanisms and radiation from other structural elements. Nevertheless, it is one important portion of the picture that will ultimately be pieced together as further research into the origin of wheel/rail noise is conducted.

The picture we present is far from complete. Nevertheless, even at this stage, many qualitative conclusions can be made which

will enhance our understanding of the role of the rail in wheel/rail noise.

2. THE WHEEL/RAIL INTERACTION

To determine how wheel and rail roughness generate vibration, consider a smooth wheel moving along a rail at constant velocity V . If the wheel encounters a bump on the rail, the wheel will be deflected upwards and the rail downwards by amounts which depend on the size of the bump and the wheel and rail resistance to motion (impedance). Assuming that wheel/rail contact is maintained, the sum of wheel and rail displacement is equal to the height of the bump.

To extend this concept to the general case of a rough wheel rolling along a rough rail, consider Fig. 1. The roughness of the wheel and rail are shown as (exaggerated) perturbations of a smooth circular wheel and smooth rail surface. At any instant, the vertical position of the wheel reference circle y_w depends on the position y_r of the rail and on the wheel and rail roughness, w and r , measured with respect to the smooth wheel and rail reference lines:

$$y_w = y_r + r + w . \quad (1)$$

Differentiating both sides of Eq. 1 with respect to time and defining wheel velocity V_w as positive upwards and rail velocity V_r as positive downwards* we can obtain a relationship between wheel and rail velocity and the rate of change of wheel and rail roughness due to motion of the contact point

$$V_w + V_r = \dot{r} + \dot{w} . \quad (2)$$

If the roughness on the wheel and rail is a sinusoidal function of frequency ω , then the vertical force $F(\omega)$ at the wheel/rail interface can be related to the wheel and rail velocities as

$$F(\omega) = Z_w V_w = Z_r V_r , \quad (3)$$

where Z_w and Z_r denote the point impedances of the wheel (connected to the vehicle) and rail (*in situ*), at frequency ω , respectively.

Solving Eqs. 4 and 5 for the interaction force and resulting wheel and rail velocities at the contact point in terms of the roughnesses, we obtain

$$F(\omega) = \frac{Z_r Z_w}{Z_r + Z_w} [\dot{r}(\omega) + \dot{w}(\omega)] , \quad (4)$$

*These directions are chosen to coincide with the directions of the vertical wheel/rail interaction forces that act on the wheel and rail, in order to facilitate the subsequent analysis.

$$V_W(\omega) = \frac{Z_R}{Z_R + Z_W} [\dot{r}(\omega) + \dot{w}(\omega)] , \quad (5)$$

and

$$V_R(\omega) = \frac{Z_W}{Z_R + Z_W} [\dot{r}(\omega) + \dot{w}(\omega)] . \quad (6)$$

The rail roughness is, in fact, a random variable and may justifiably be characterized as a stationary random process with a wavenumber spectrum $\phi_{rr}(k)$. Here k denotes wavenumber. In the absence of experimental data, it is not clear how best to characterize the wheel roughness. If the roughness were uniform across the running surface but varied circumferentially, it would be characterized completely by a Fourier series. However, if lateral profile variations are significant, the circumferential roughness pattern would not necessarily be repetitive as the wheel oscillates laterally over a rail which will itself contain lateral irregularities. Accordingly, we shall also model the wheel roughness as a stationary random function. This allows us to write a simple expression for the relationship between the frequency spectra of interaction force and wheel and rail velocity and the frequency spectra of wheel and rail roughness velocity.*

*The spectrum $\phi_{dd}(\omega)$ of a dependent variable is related to the spectrum $\phi_{ii}(\omega)$ of an independent variable by $\phi_{dd}(\omega) = |H(\omega)|^2 \phi_{ii}(\omega)$ where $H(\omega)$ is the transfer function relating to two variables. Equations 4, 5, and 6 provide us with the required transfer functions as ratios of the wheel and rail impedance.

However, the frequency spectrum of wheel and rail roughness velocity is, of course, dependent on the speed with which the wheel travels over the rail. It is more convenient to deal with an invariant measure of the roughness. Such a measure is the *wave-number* spectrum of the *magnitude* of the roughness.

The relation between a frequency and wavenumber spectrum is given by

$$\Phi_{tt}(\omega)d\omega = \Phi_{xx}(k)dk . \quad (7)$$

Equation 7 reflects a requirement for equal mean square values in corresponding frequency and wavenumber bands. Since $\omega = kV$, where V is vehicle velocity,

$$\Phi_{tt}(\omega) = V^{-1}\Phi_{xx}(k) . \quad (8)$$

Noting also that a velocity spectrum is simply ω^2 times the displacement spectrum, we may apply Eq. 8 along with the general relation between an input and output spectrum to Eqs. 4 - 6 to obtain

$$\Phi_{FF}(\omega) = \frac{\omega^2}{V} \left| \frac{Z_r Z_w}{Z_r + Z_w} \right|^2 [\Phi_{rr}(k) + \Phi_{ww}(k)] , \quad (9)$$

$$\Phi_{V_w V_w}(\omega) = \frac{\omega^2}{V} \left| \frac{Z_r}{Z_r + Z_w} \right|^2 [\Phi_{rr}(k) + \Phi_{ww}(k)] , \quad (10)$$

and

$$\phi_{V_R V_R}(\omega) = \frac{\omega^2}{V} \left| \frac{Z_W}{Z_R + Z_W} \right|^2 [\phi_{RR}(k) + \phi_{WW}(k)] . \quad (11)$$

At first glance, Eqs. 9 - 11 seem to suggest that at a given frequency the force and velocity spectra decrease with increasing vehicle velocity. We know that this is not the case and, in fact, a careful look at these equations shows that they imply no such thing. Recalling that $k = \omega/V$, we can see that at a given frequency an increase in velocity implies a decrease in wavenumber. As a result, how the spectra of interaction force and wheel and rail velocity vary with velocity depends intimately on the character of the wheel and rail roughness. We will discuss this question in somewhat more detail below.

Equations 9, 10, and 11 represent a general formula for the vertical forces and motion at the wheel/rail interface due to wheel/rail roughness. A complete evaluation requires data on wheel and rail roughness wavenumber spectra and analytical and experimental formulations of Z_W and Z_R . Although rail spectral data have been acquired [1], the wavenumber range is far too low for purposes of noise calculation. To apply to vehicles traveling at, say, 100 ft/sec, over a frequency range from 100 - 5000 Hz these data must span a wavenumber range from about 6 - 300 rad/ft. This corresponds to wavelength of .02 - 1 ft. Presently, rail and wheel spectral data valid over this region are not

extant but are sorely needed. Without such data, absolute levels cannot be predicted; however, the effect of modifications to existing systems may be interpreted with Eqs. 9 - 11, once Z_w and Z_r are characterized.

3. WHEEL AND RAIL RESPONSE

3.1 Theoretical

The impedance Z_w of the train looking into the wheel depends at low and high frequencies on construction details but is likely to be rather independent of such details over a mid-frequency regime. Axles are generally mounted to truck frames with springs on rubber bushings which isolate the frame from the wheel set. Springs can become effective at frequencies under 10 Hz, whereas rubber bushings do not take effect until about 30 - 50 Hz. Accordingly the wheel behaves as a rigid mass above roughly 50 Hz and below the first resonance which occurs at several hundred Hz. Thus, a reasonable first approximation for Z_w is

$$Z_w = j\omega M, \quad (12)$$

where M is the mass of the wheel, bearing, and an equivalent axle mass.* A wheel typically weighs 800 lbs and an axle 820 lbs.

*Viewing the axles as a rigid beam, pivoted about one end, this equivalent mass is one third of the total axle mass.

Thus, the parameter M in Eq. 12 is expected to be in excess of 1000 lbs.

Whether mounted on tie and ballast or to a rigid foundation by means of resilient fasteners, a rail may reasonably be modeled as a beam on an elastic foundation. The response to a localized excitation at the wheel/rail interface is rather straightforward, and existing derivations are readily available [2,3,4]. Here we will interpret the expressions for the complete rail response and for the impedance.

The spatial part of the rail response for $x \geq 0$ to a harmonic force F at frequency ω may be viewed in the following form that is readily amenable to interpretation:

$$y(x) = \frac{\sqrt{2}F e^{-k_r x/2}}{4EI k_r^3} \left[\cos\left(\frac{k_r x}{\sqrt{2}}\right) + \sin\left(\frac{k_r x}{\sqrt{2}}\right) \right] \quad f \leq f_0 \quad (13)$$

$$y(x) = \frac{F}{4EI k_r^3} \left(j e^{jk_r x} - e^{-k_r x} \right) \quad f \geq f_0 \quad (14)$$

Here $k_r = |K/EI (\omega^2/\omega_0^2 - 1)|$, K is the fastener stiffness per unit length of rail, E = Young's modulus, I = the moment of inertia, and $f_0 = 1/2\pi \sqrt{K/\rho_0}$ is the natural frequency of the rail acting as a rigid body on the fastener. Equations 13 and 14 are sketched in Fig. 2. At frequencies below f_0 , there is only a

structural nearfield associated with the rail; at higher frequencies, both near and far fields are present. For typical rail systems, f_0 lies somewhere between 50 and 300 Hz.

The rail impedance is found by differentiating Eqs. 13 and 14 with respect to time to obtain the vertical rail velocity, and evaluating the ratio $F/\dot{y}(0)$. The results are

$$Z_r = j2\sqrt{2}(EI)^{\frac{3}{4}}K^{\frac{3}{4}}\omega^{-1} [1 - (\omega/\omega_0)^2]^{\frac{3}{4}} \quad \omega \leq \omega_0 \quad (15)$$

$$Z_r = 2(EI)^{\frac{3}{4}}K^{\frac{3}{4}}\omega^{-1} \left[\left(\frac{\omega}{\omega_0} \right)^2 - 1 \right]^{\frac{3}{4}} (1 - j) \quad \omega \geq \omega_0 \quad (16)$$

3.2 Experimental Determination of Rail Impedance

In order to give ourselves some confidence in the simplified model of rail impedance above, we measured the mechanical impedance of an AREA 100 rail resiliently mounted (NYCTA fasteners with a stiffness of 5×10^5 lb/in.) in an operational New York City Transit Authority roadbed using a vibration generator and an impedance head as shown in Fig. 3. The measurement was made in the vertical direction normal to the surface of the rail.

A small plate containing a stud was glued to the rail head. To this stud we attached an impedance head (for measuring the applied force) and shaker. A separate accelerometer attached

directly to the rail head was used to measure the acceleration at the forcing point. The shaker was excited with 1/10 octave bands of noise in the frequency range from 40 to 6300 Hz. By recording the amplitude of the force and acceleration and the phase between them (using a polarity coincidence correlator), we were able to obtain the rail impedance shown in Fig. 4. The agreement of the measurements with the theory of Eqs. 15 and 16 is seen to be very good up to about 2000 Hz.

The amplitude of a phase measurement reflects the presence of damping in the rail fasteners which is not accounted for by the theory. As a result, there is some discrepancy between theory and measurement near the resonance frequency.

At very low frequencies (below the resonance frequency f_0) the rail impedance is controlled by the stiffness of the rail fastener and, hence, decreases like $1/\omega$. At the resonance frequency, the mass impedance of the rail cancels the stiffness impedance of the fasteners, resulting in a strong minimum. At high frequencies, the rail moves essentially independently of the fastener stiffness and for all practical purposes is essentially a freely vibrating beam with the impedance increasing like $\omega^{3/2}$. Measurements by other investigators [5,6] have shown similar results.

3.3 Comparison of Wheel and Rail Impedance

A plot of Z_w and Z_r for a range of values of f_0 and for an effective wheel mass of 1000 lbs is shown in Fig. 5. The curve for Z_r applies to AREA 100 rail. This plot shows that above about 100 Hz $Z_r \ll Z_w$. Accordingly, the wheel acts largely as a velocity source and the rail motion is largely independent of wheel or rail impedance. As a result the equation of the spectra of interaction force and wheel and rail velocity (Eqs. 9 - 11) simplify to

$$\Phi_{FR}(\omega) = \frac{\omega^2}{V} |Z_r|^2 [\Phi_{rr}(k) + \Phi_{ww}(k)] \quad (17)$$

$$\Phi_{V_w V_w}(\omega) = \frac{\omega^2}{V} \left| \frac{Z_r}{Z_w} \right|^2 [\Phi_{rr}(k) + \Phi_{ww}(k)] \quad (18)$$

$$\Phi_{V_r V_r}(\omega) = \frac{\omega^2}{V} [\Phi_{rr}(k) + \Phi_{ww}(k)] \quad (19)$$

Equations 18 and 19 imply that the local response of the wheel (at the point of contact) is much less than the rail response at that point. However, this does not necessarily imply that that radiation from the rail will dominate the noise from wheel/rail interaction. Whether the wheel or the rail dominates will depend on such considerations as the radiation efficiency of the wheel and the rail, how fast the rail vibration dies out as one moves away

from the excitation point, and possibly the location of the observer. Equation 19 implies that the rail response is largely independent of the wheel or rail impedance. We will use this fact in the next section to estimate the spectrum of roughness on the wheel and rail.

4. ESTIMATION OF THE ROUGHNESS SPECTRUM

Although there are no data extant, we can obtain an order-of-magnitude estimate of the combined wheel/rail roughness from rail vibration data. Recalling that the acceleration spectrum is simply ω^2 times the velocity spectrum, Eq. 19 can be solved for the combined wheel/rail roughness wavenumber spectrum as a function of the rail acceleration spectrum $\phi_{a_r a_r}(\omega)$:

$$\phi_{rr}(k) + \phi_{ww}(k) = \frac{V}{\omega^4} \phi_{a_r a_r}(\omega) . \quad (20)$$

A 1/3-octave band spectrum of rail vibration taken on NYCTA tracks is shown in Fig. 6. The train was passing at approximately 32 ft/sec. By processing the data using Eq. 20 we obtain the 1/3-octave band wavenumber spectrum of Fig. 7. The roughness amplitude at the shortest wavelength of interest - i.e., the length of the contact zone, approximately 1/2 in. is ~30 micro-inches. For wavelengths greater than 4 in., Eq. 20 is no longer

valid, since the wavelength implies a frequency of approximately 100 Hz in the acceleration data, and at that frequency the wheel and rail impedances are becoming comparable. The rms roughness amplitude at this upper bound in wavelength is about 1 mil. Although this calculation is crude, it has given us some indication of the roughness amplitudes we can expect, and it also shows us that the roughness spectrum decreases as the fourth power of the wavenumber. If we substitute this fourth power dependence of the roughness spectrum into Eqs. 17, 18, and 19, we obtain

$$\phi_{FF}(\omega) = c \frac{V^3}{\omega^2} |Z_R|^2 \quad (21)$$

$$\phi_{V_W V_W}(\omega) = c \frac{V^3}{\omega^2} \left| \frac{Z_R}{Z_W} \right|^2 \quad (22)$$

$$\phi_{V_R V_R}(\omega) = c \frac{V^3}{\omega^2} \quad (23)$$

This model then implies that the interaction force and wheel and rail velocity spectra will increase as the third power of the velocity. It is a commonly observed fact that the sound pressure level generated by train passages (wheel/rail noise) does, in fact, vary as 25 to 30 times the logarithm of the velocity, which agrees well with the above model.

5. RAIL RADIATION

So far we have considered in some detail the rail response to the microroughness on the wheel and the rail. Of equal importance is the efficiency with which this dynamic response is transformed into acoustic radiation. In this section we describe an analytical/experimental study of rail radiation efficiency.

A rail will radiate sound from the structural nearfield and from free bending waves that travel at supercritical velocities, i.e., waves whose propagation velocity exceeds the velocity of sound. The frequency regime of greatest interest in the radiated noise spectrum (above several hundred Hz) is generally above the rail natural frequency f_0 . Accordingly, there will always be free bending waves which, if supercritical, will be the dominant source of noise. Calculation of the propagation speed of bending waves on a rail with a resilient fastener of zero stiffness indicates that for rails from light (AREA 90)* to heavy (AREA 133), the frequency above which these waves are supercritical varies from 55 to 65 Hz - far below the region of interest. The additional stiffness of actual elastic rail fasteners increases the bending wave speed at a given frequency. Accordingly, the

*AREA denotes an American Railway Engineers Association designation. The accompanying number is the weight of the rail (in pounds) per yard of length.

frequency range represents an upper bound for the critical frequency of resiliently supported rails.

An analytical description of the radiation from an object with a shape as complicated as that of a rail is not easily obtained, at least until we have a better understanding of how the rail responds to excitation from interaction with the wheel.

5.1 Rail Response

To examine the rail response to point excitation simulating its interaction with a wheel, we performed measurements on a 20 ft section of AREA-100 rail. The rail was supported every 2 ft along its length by resilient pads which in turn rested on a concrete floor. No attempt was made to simulate the stiffness of resilient fasteners used in transit authority operations, because in the frequency range of interest for acoustic radiation, the rail responds essentially independently of the fastener stiffness (see Sec. 3). The rail was excited by a 50-lb capacity electronic shaker attached to the rail head. The shaker was oriented to force the rail vertically (such as one would expect from micro-roughness or impact at joints), and then by attaching the shaker to the side of the rail head, we excited the rail horizontally (such as would result from flange impact). The rail response was measured at 5 positions on the head, 5 positions on the web, and 5 positions on the foot.

The rail response (a 5-point spatial average) on the head, web, and foot* for vertical excitation is shown in Fig. 8. The vertical acceleration of the head and foot are essentially the same up to 3000 Hz and the web acceleration in the horizontal direction normal to the plane of the web is negligible to beyond 4000 Hz. This implies that the rail moves essentially as a simple beam. At about 3000 to 4000 Hz is an apparent resonance of the foot on the web stiffness in which the foot response exceeds the head response by about 5 dB.

The rail acceleration for horizontal excitation of the rail head is shown in Fig. 9. The horizontal acceleration of the head and the web are essentially the same up to 2500 Hz, and the foot response is negligible up to about 2000 Hz. Except for a peak at 3150 Hz, where the foot response dominates, the head, web, and foot respond essentially the same up to 5000 Hz where the web begins to dominate the response. This response pattern is somewhat more complicated than for vertical forcing; however, at low frequencies the pattern that the head and web respond and the foot remains essentially stationary is as one would expect from the geometry of the forcing.

*For all measurements, the accelerometer was located in the center of the web for web acceleration and halfway between the web and the edge of the foot for the foot accelerations (see Figs. 8 and 9).

5.2 Radiation Efficiency: Theoretical

With a clearer understanding of how the rail responds to the anticipated forcing during wheel/rail interaction, we are in a better position to discuss the anticipated radiation characteristics. Recall that the radiation efficiency σ is defined as

$$\sigma = \frac{\pi}{\rho c A \langle v^2 \rangle}, \quad (24)$$

where π is the time averaged acoustic power radiated, ρc is the acoustic impedance, A is the area from which the object radiates and $\langle v^2 \rangle$ is the mean squared, space-time averaged velocity of the radiating surface of the object. From the response measurements in Sec. 5.1 we make the crude approximation that for vertical forcing the head and foot respond the same and dominate the response. For horizontal forcing we make the crude approximation that only the head and web respond and that they respond the same. These crude approximations will, of course, lead to errors at high frequencies. But at this state we want to make as simple a model as possible. Refinements can be added as required.

To estimate the radiation efficiency, we treat the rail as a cylinder. Formulations for the radiation efficiency of a cylindrical cross section beam have been calculated by Bailey and Fahy [7] under the good assumptions that the beam is above the coincidence frequency (supercritical bending wave speeds) and that it

is long compared to an acoustic wavelength. The expression for the radiation efficiency is

$$\sigma = \frac{\eta}{\rho c (2r) L \langle v^2 \rangle} = \{kr [|J_1'(kr)|^2 + |Y_1'(kr)|^2]\}^{-1}, \quad (25)$$

where r is the beam radius, L is the length, k is the acoustic wavenumber, J_1 and Y_1 are Bessel functions of the first and second kind respectively of order 1, and

$$J_1'(z) = \frac{\partial}{\partial z} J_1(z), \text{ etc.}$$

We apply Eq. 25 to calculate the rail radiation efficiency for the horizontal forcing of the rail by taking the cylinder diameter equal to the rail height (Eq. 26 with $r = \text{rail height}/2 = 3 \text{ in.}$). For the vertical forcing of the rail, we model the rail as two cylinders vibrating independently such that the power radiated is the sum of that radiated from each. The diameter of one cylinder equals the rail head width (2-11/16 in.), and the diameter of the second equals the rail foot width (5-3/8 in.). The resulting expression for the radiation efficiency becomes

$$\sigma_{\text{vertical forcing}} = \frac{\sigma(r_H)r_H + \sigma(r_F)r_F}{r_H + r_F}, \quad (26)$$

where $\sigma(r_F)$ is Eq. 26 evaluated for $r = r_F$ and r_H is half the rail width and r_F is half the rail foot width. We will compare these approximations with measured results in the next sections.

5.3 Radiation Efficiency: Measured

To measure the rail radiation efficiency for comparison with the simple theoretical models discussed in Sec. 5.2, the same 20-ft section of AREA-100 rail was mounted as described in Sec. 5.1 in a reverberant chamber (~4000 cu ft). The chamber was calibrated so that the power radiated by the rail could be inferred by measuring the sound pressure level in the chamber. The rail was excited as described in Sec. 5.1 at the rail head in both the vertical and horizontal directions. The sound pressure level in the room was monitored at three positions and a mode mixer was employed to enhance the reverberant character of the room. By enclosing the shaker in a box (3/4 in. plywood walls) lined with 2 in. of fiberglass, we were able to ensure that the noise from the shaker was more than 16 dB below the noise from the rail for all frequencies above 200 Hz.* The rail response was measured as described in Sec. 5.1, and the levels obtained were the same as those shown in Figs. 8 and 9.

In order to reduce the data by means of Eq. 24, we require the mean square rail velocity $\langle v^2 \rangle$, the time averaged sound power

*This comparison was made by connecting the shaker to a very short section of rail, so that both shaker and rail were enclosed within the box. By operating the shaker at the same current level as when attached to the full rail and measuring the SPL in the room, the noise from the shaker could be assessed.

radiated π , and an appropriate measure of the radiating area of the rail. For both vertical and horizontal forcing of the rail, we take $\langle v^2 \rangle$ to be the space averaged rail head velocity. For vertical excitation, the area A is taken as the sum of the rail head and rail foot widths times the rail length, and for horizontal excitation A is the rail height times the rail length. The sound power is, of course, obtained from the room characteristics and the average of the SPL measured at the three points in the room. A comparison of these measurements with the theoretical calculations of Sec. 5.2 is shown in Figs. 10 and 11.

For vertical excitation, the agreement between theory and measurement in Fig. 10 is quite good, except in the vicinity of 5000 Hz, where the fact that the foot response dominates the head response tends to make measured estimates of σ based on the head response too high. Note that at high frequency the theoretical estimate of σ tends to be 2 dB (the cylinder radiates from both sides) and that in general the measured radiation efficiency is somewhat greater than the theoretical estimates, suggesting that the theory would tend to underestimate the rail radiation.

For horizontal excitation, the agreement between theory and measurement is again good. In the 2500 to 4000 Hz range the measured values are high, because the foot response dominates at these frequencies and basing the calculation of σ on the head response tends to overestimate the radiation efficiency.

We see then that rails are very efficiency radiators of acoustic energy above 500 Hz, coinciding well with those frequencies to which the ear is sensitive. However, by referring to Eq. 23, we see that it is anticipated that the rail response will fall with the square of frequency. Thus, reduced rail response at high frequencies will tend to mitigate efficient radiation there.

The whole picture is still not complete. For example, we still require the length of rail that participates in the radiation. Rail joints, highly damped rail fasteners, and damping due to the ballast may all tend to reduce the rail vibration as one moves along the rail and away from the excitation point. The shorter the length of rail effectively vibrating the less acoustic power is radiated. Some data from Naake [5] suggests that with jointed rail the rail length is generally on the order of one rail segment (39 ft), but further work is required.

5.4 Comparison With Measured Wheel/Rail Noise

It is interesting to compare the predicted noise level that will be radiated by a rail according to the analytical model in Fig. 10 with the noise actually measured during a train passage. To do this, during a train passage we take measurements of rail acceleration at the rail foot and sound radiated at 75 ft away.*

*The measurements were made on the Staten Island Railroad (welded rail) during February 1972.

Using the acceleration measurements, treating the rail as a line source, taking the rail characteristics of an AREA-100 rail, and assuming uniform directivity, we can predict by the analytical model of Fig. 10 the anticipated rail radiation. Comparing these predictions with the noise measurements show how much the rail contributes to the radiation. Figure 12 shows that the rail apparently contributes significantly only in a few bands (500 - 800 Hz and 5000 - 6300 Hz). Other sources, such as the wheel, must be dominant in the other bands.

The results here should, of course, be viewed with some caution. For example, we have neglected the directivity of the rail and have assumed that an infinite length of rail participates in the radiation. If the rail is vibrating primarily in the vertical direction, then these approximations are conservative, i.e., predicting more rail noise than actually occurs. If, however, the rail also vibrates in the horizontal direction with an acceleration level the same as that in the vertical direction, then we may be underestimating the radiation by an amount that depends on the directivity. In general though, the large difference in measured and predicted SPL suggests that the rail is a small contributor to the sound radiation in 1000 to 4000 Hz range.

6. CONCLUSIONS

The influence of rails on train noise has been examined with particular reference to noise generated by microroughness on wheels and rails. By modeling the wheel as a simple mass, we showed that the wheel impedance is generally greater than the rail impedance, implying that wheel response should be less than rail response. Further, it has been found that the rail impedance is well modeled by a simple beam on an elastic foundation and that it is an efficient radiator above 500 Hz, with a radiation efficiency that can be well-modeled by the uniform notion of simple cylindrical beams. The roughness spectrum on wheels and rails has been estimated and shown to decrease with increasing wave-number, like k^{-4} , leading to the well-known $30 \log V$ wheel/rail noise velocity dependence.

It should be emphasized that the role of the rail in wheel/rail noise is far from completely understood; several important pieces of information are still missing. For example, the length of rail that effectively radiates when excited by the passage of the wheel as well as the directivity pattern of the radiation are currently unknown, and no measurements exist to define the roughness spectrum on wheels and rails. With respect to the wheel, we have assumed a very simple model of the impedances (a mass) when in fact we know that the wheel is a resonant structure in the

frequency range of interest. If these resonances are lightly damped, they can strongly reduce (or increase) the impedance, seriously affecting our model of the wheel/rail interaction. As a result, the wheel impedance needs to be measured and modeled. Of course a complete picture of wheel/rail interaction would also require a detailed understanding of the response and radiation characteristics of the wheel as well as other mechanisms of noise production, such as squeal and impact, but these are beyond the scope of this paper.

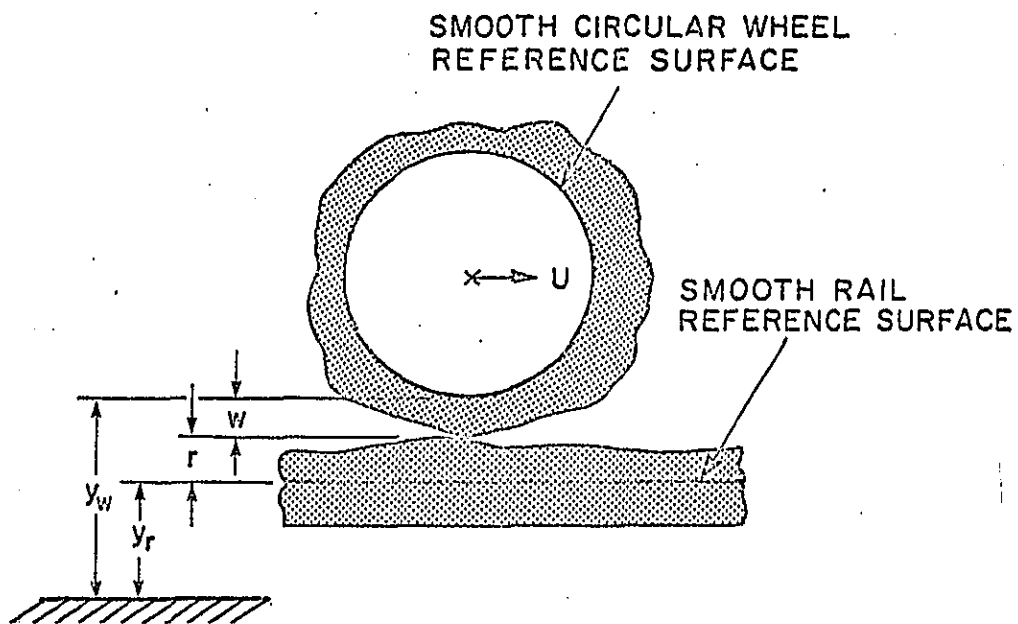
REFERENCES

1. A.O. Gilchrist, "A Report on Some Power Spectral Measurements of Vertical Rail Irregularities", British Railway Research Dept., Derby, England (1965).
2. S. Timoshenko, "Methods of Statistical and Dynamical Stresses in Rails", *Proceeding of the 2nd International Congress for Technical Mechanics*, Zurich (1926), p. 407.
3. J. Dörr, "Infinitely Resiliently Supported Beams Excited by an Evenly Proceeding Load", *Z. Ing. Archiv.* XIV, No. 3 (1943), pp. 167-192.
4. J. Dörr, "The Dynamics of a Resiliently Supported Infinite Beam", *Z. Ing. Archiv.* XIV, No. 5 & 6 (1948), pp. 287-298.
5. H.J. Naake, "Experimental Investigation of the Dynamical Behavior of Railroad Tracks", *Acoustika* 3 (1953), p. 139.
6. G. Jolberg, "Vibration Measurements on Various Railroad Tracks", *Proceeding of the Conferences on Akustik and Schwingungs Technik*, Stuttgart (1972).
7. J.R. Barley and F.J. Fahy, "Radiation and Response to Cylindrical Beams Erected by Sound", *ASME Trans. J. of Engineering for Industry* 94, Series B, No. 1 (1972), pp. 139-147.

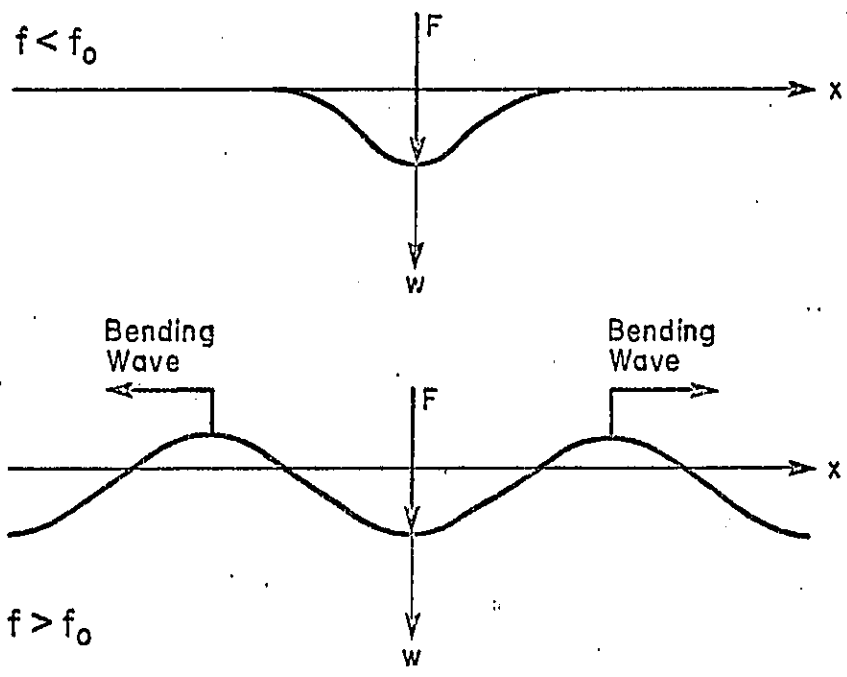
LIST OF FIGURES

- Fig. 1. Wheel and Rail Roughness Parameters.
2. Rail Response Above and Below the Resonance Frequency.
3. Rail Impedance Measurement Set-up.
4. Measured Rail Impedance.
5. Comparison of Wheel and Rail Impedances.
6. Measured Rail Vibration.
7. Wheel/Rail Roughness Spectrum.
8. Rail Response to Vertical Excitation.
9. Rail Response to Horizontal Excitation.
10. Rail Radiation Efficiency Vertical Excitation.
11. Rail Radiation Efficiency Horizontal Excitation.
12. Comparison of Predicted and Measured Rail Radiation
Due to Train Passage at 75 ft From the Track.

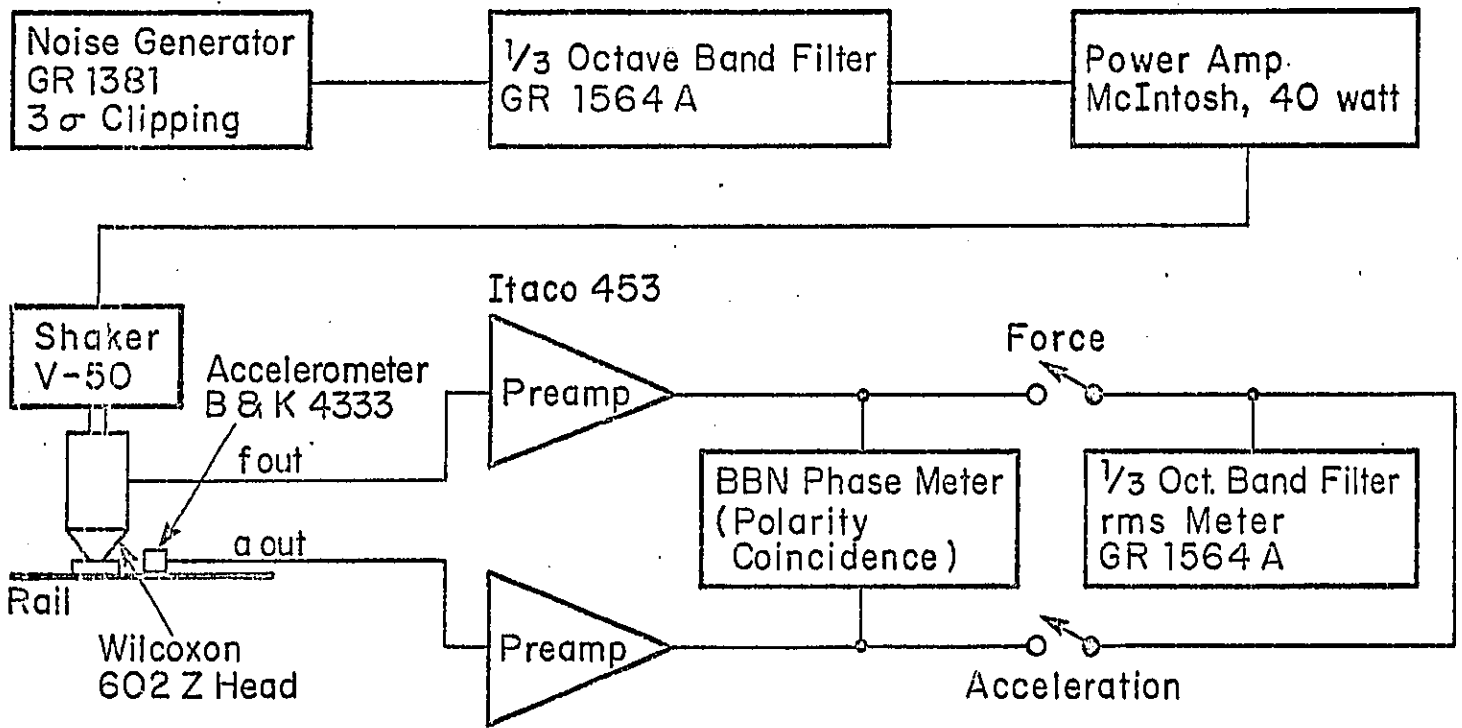
WHEEL AND RAIL ROUGHNESS PARAMETERS



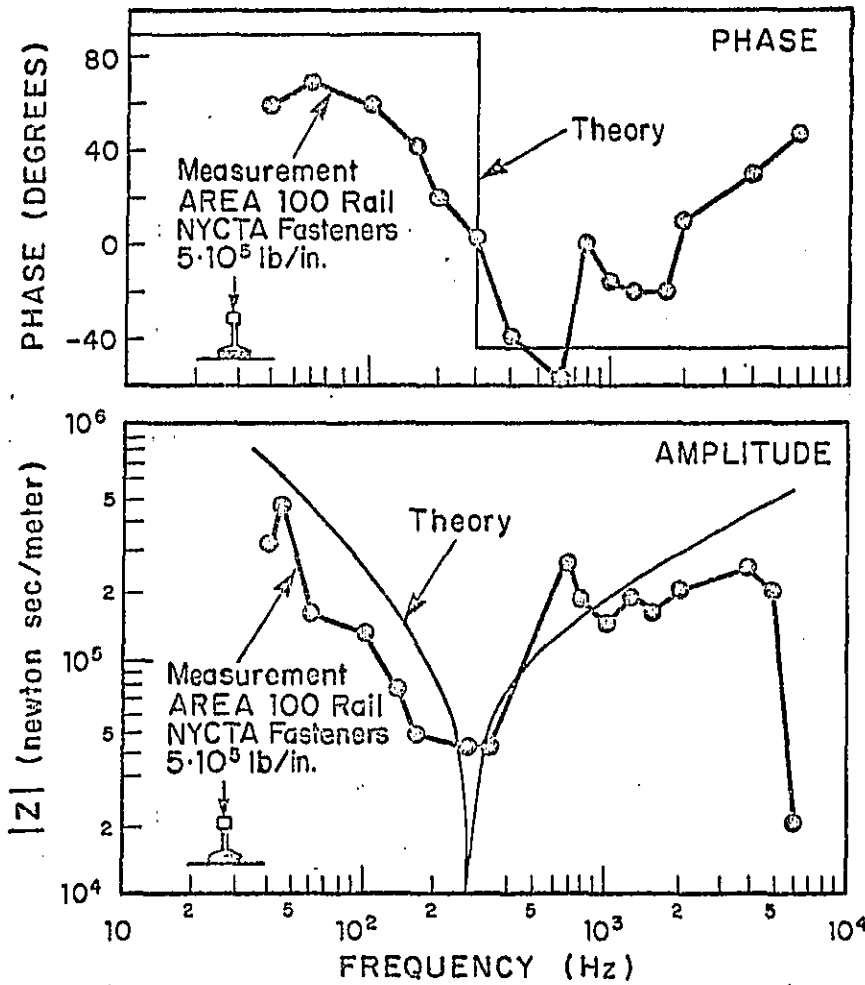
RAIL RESPONSE ABOVE AND BELOW THE RESONANT FREQUENCY f_0

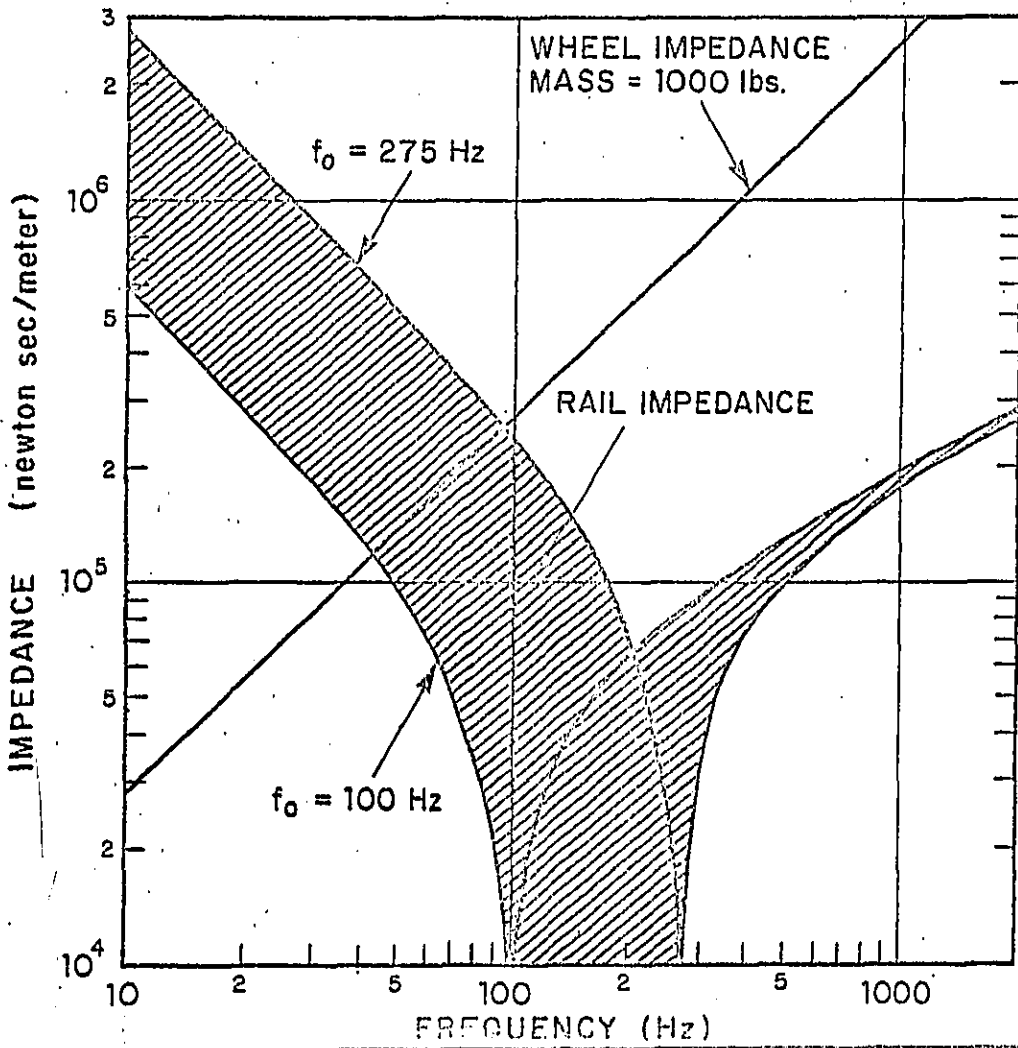


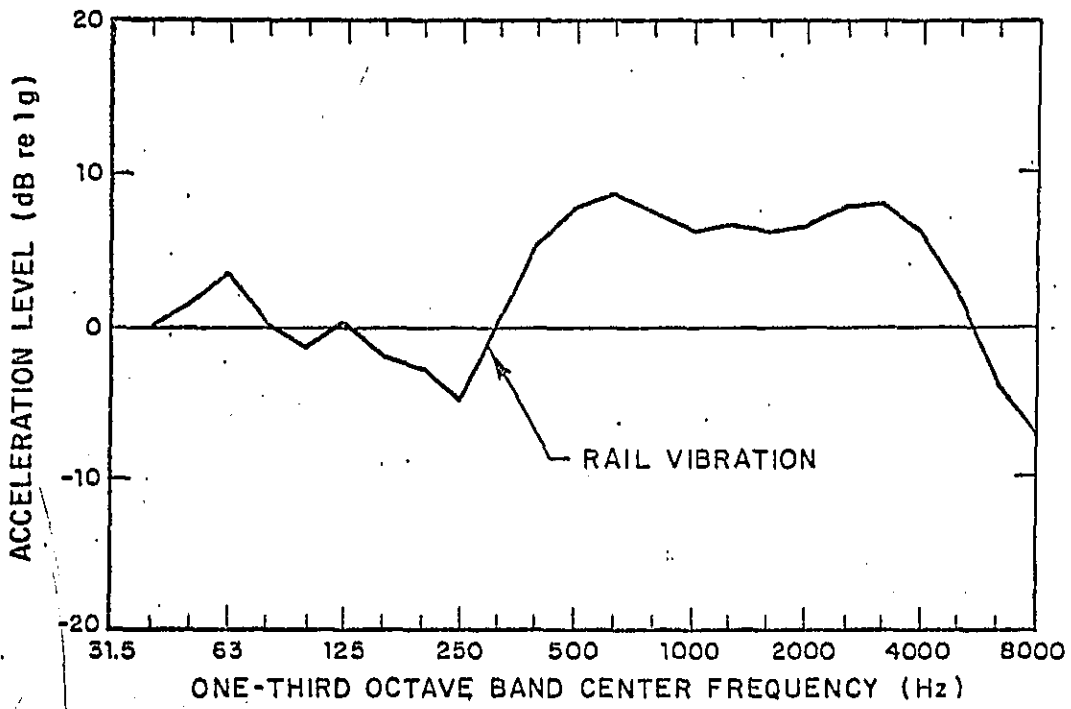
RAIL IMPEDANCE MEASUREMENT SETUP

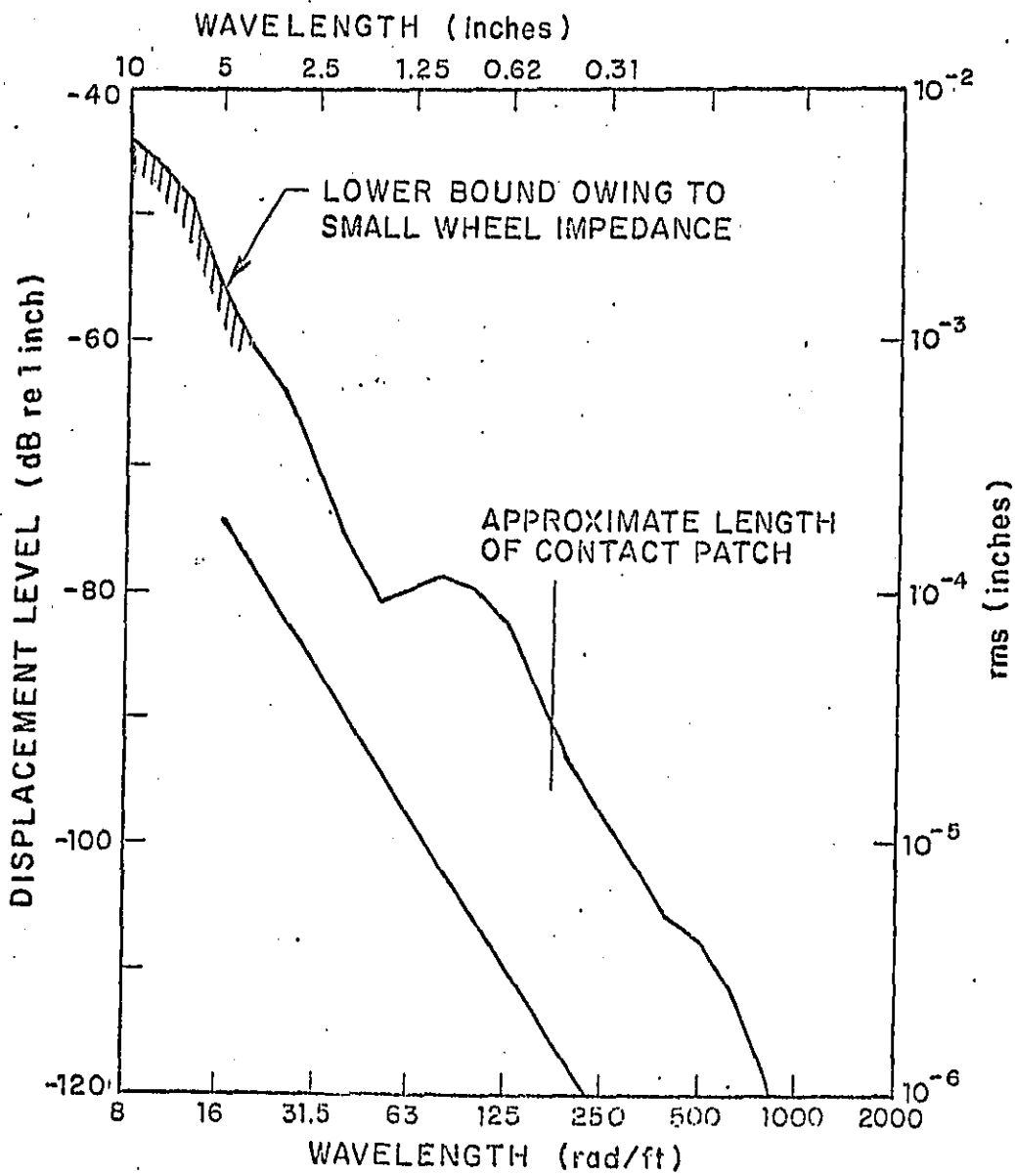


MEASURED RAIL IMPEDANCE

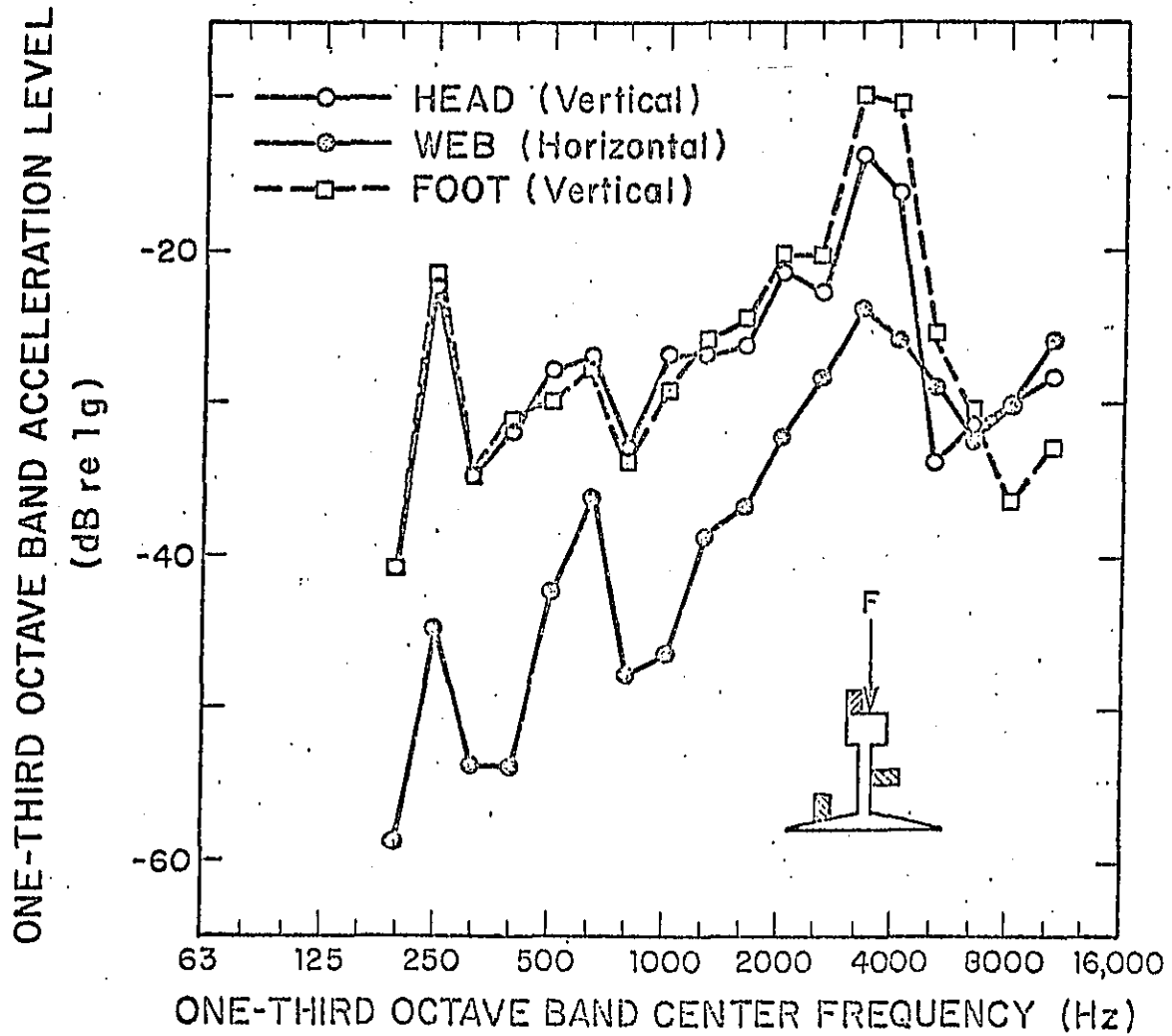




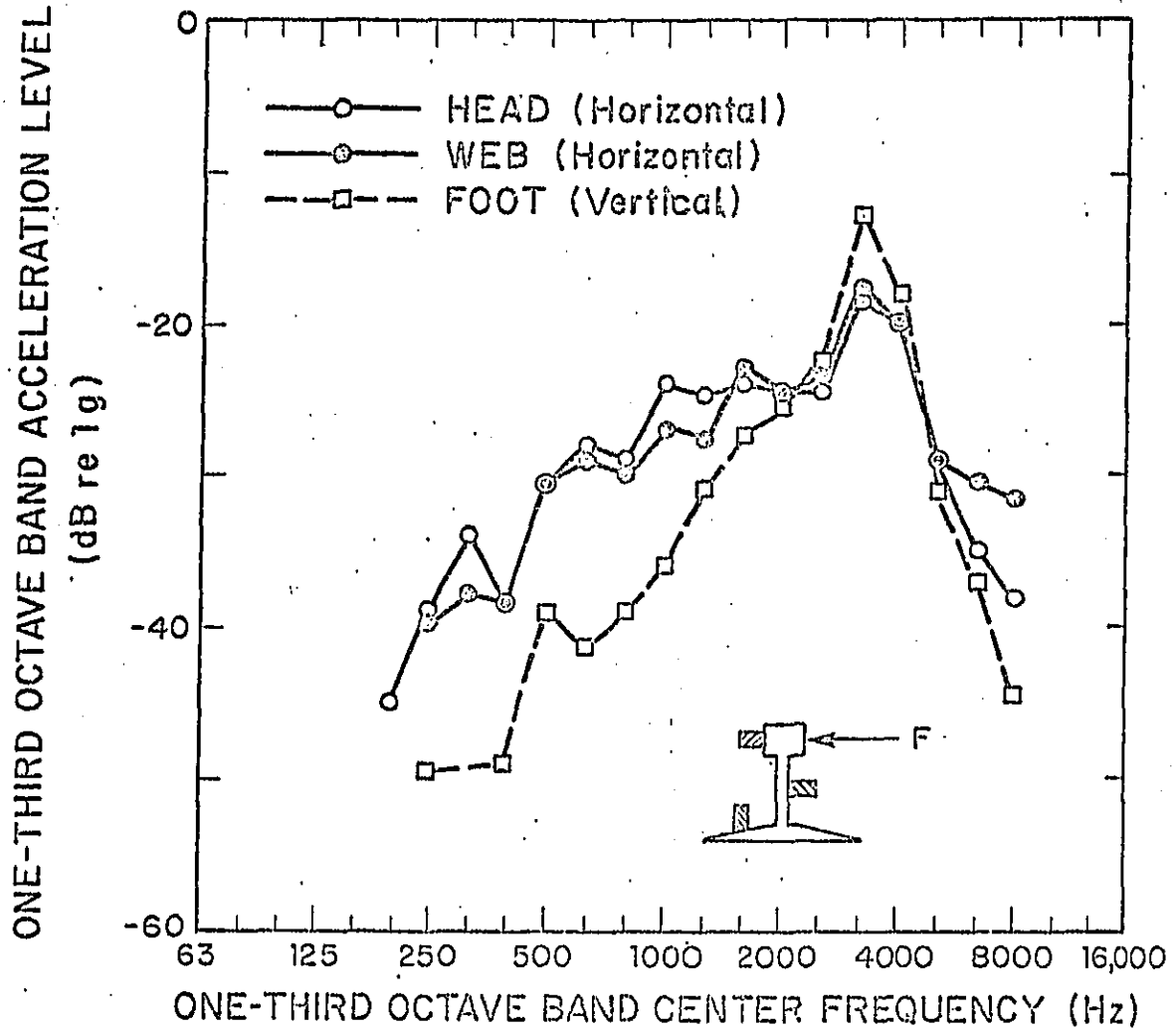




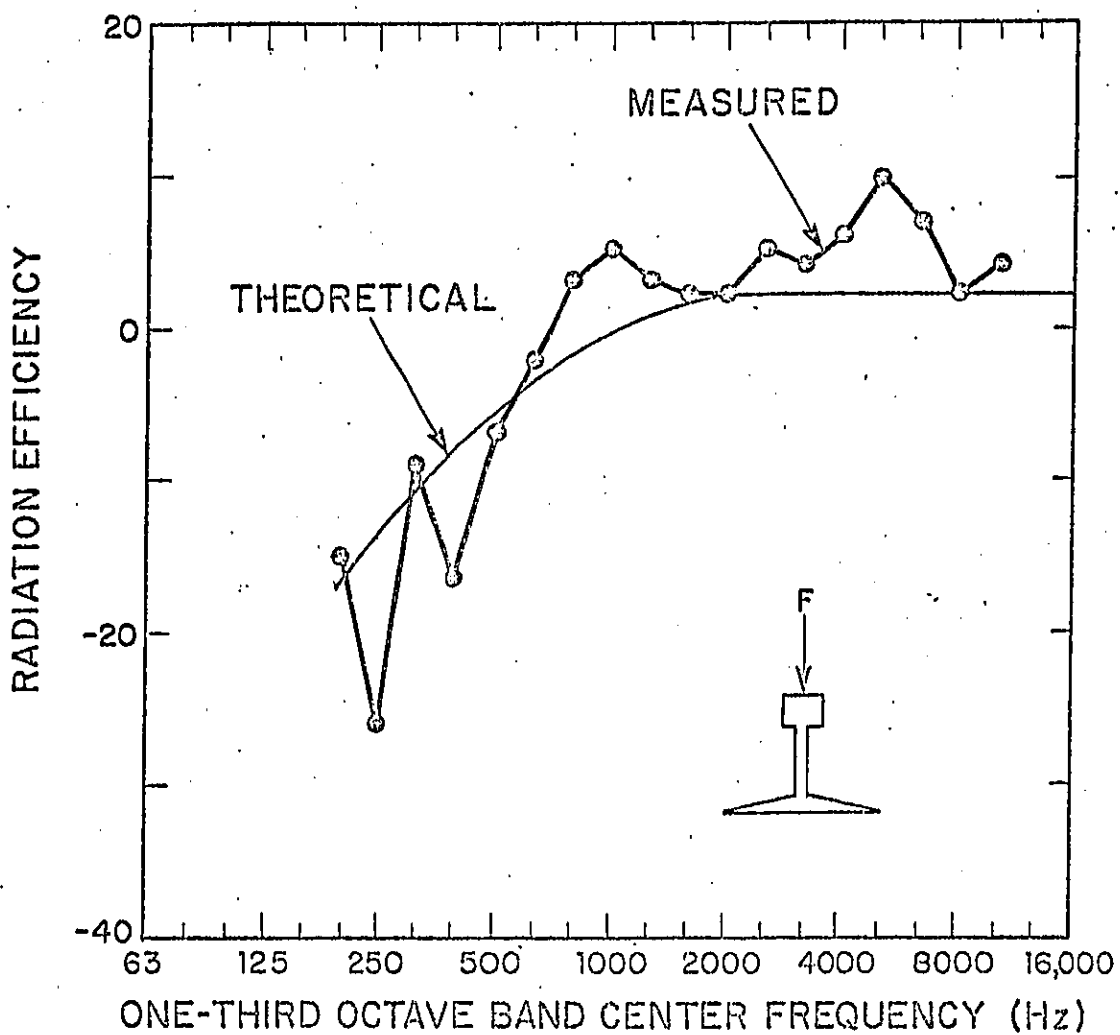
RAIL RESPONSE TO VERTICAL EXCITATION



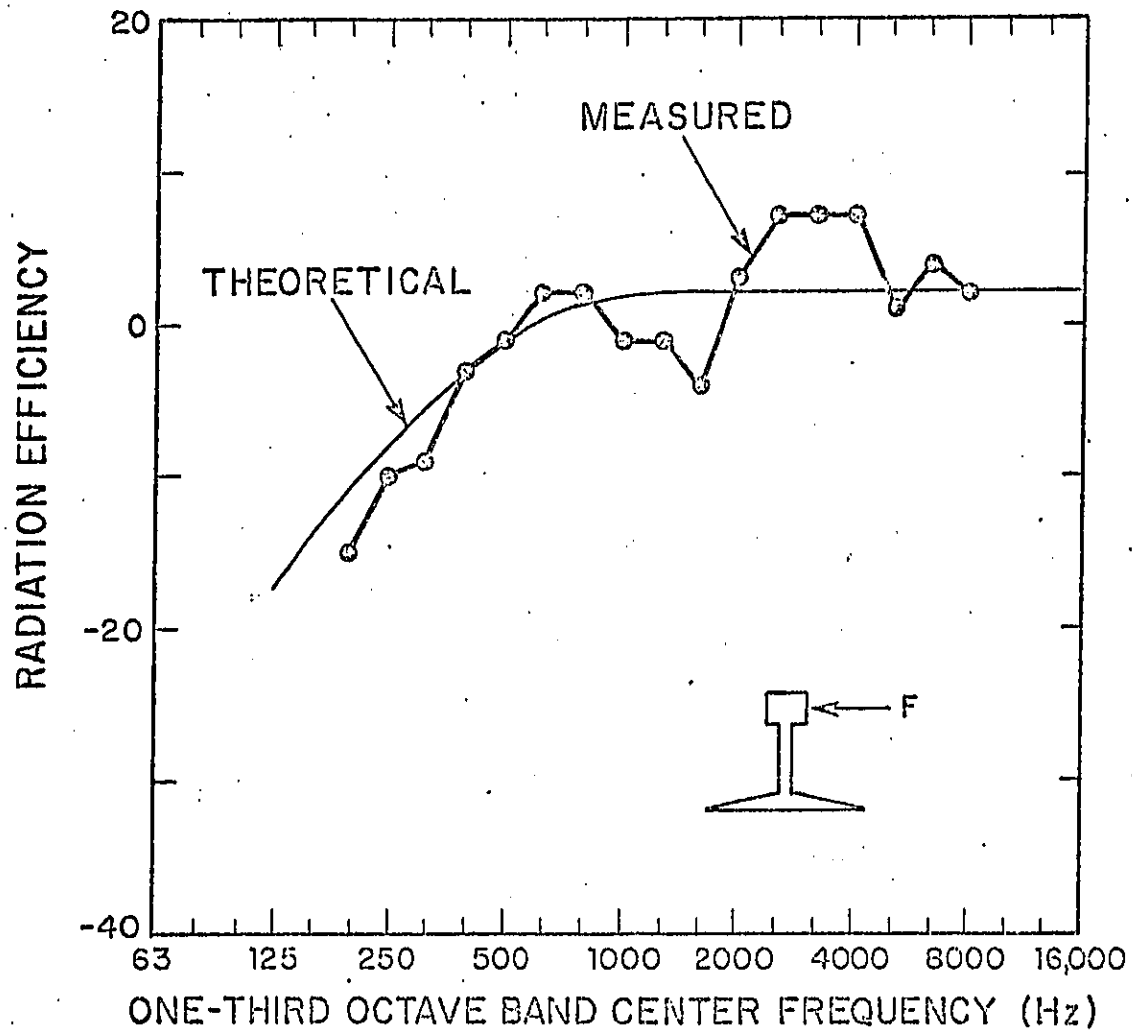
RAIL RESPONSE TO HORIZONTAL EXCITATION



RAIL RADIATION EFFICIENCY VERTICAL EXCITATION



RAIL RADIATION EFFICIENCY HORIZONTAL EXCITATION



COMPARISON OF PREDICTED AND MEASURED
RAIL RADIATION DUE TO TRAIN PASSAGE
AT 75 ft FROM TRACK

